

Range-Based Autonomous Underwater Vehicle Navigation Expressed in Geodetic Coordinates

Rami S. Jabari

Thesis submitted to the Faculty of the
Virginia Polytechnic Institute and State University
in partial fulfillment of the requirements for the degree of

Master of Science
in
Electrical Engineering

Daniel J. Stilwell, Chair
Wayne L. Neu
Craig A. Woolsey

May 6, 2016
Blacksburg, Virginia

Keywords: Autonomous Underwater Vehicle, Navigation
Copyright 2016, Rami S. Jabari

Range-Based Autonomous Underwater Vehicle Navigation Expressed in Geodetic Coordinates

Rami S. Jabari

(ABSTRACT)

Unlike many terrestrial applications, GPS is unavailable to autonomous underwater vehicles (AUVs) while submerged due to the rapid attenuation of radio frequency signals in seawater. Underwater vehicles often use other navigation technologies. This thesis describes a range-based acoustic navigation system that utilizes range measurements from a single moving transponder with a known location to estimate the position of an AUV in geodetic coordinates. Additionally, the navigation system simultaneously estimates the currents acting on the AUV. Thus the navigation system can be used in locations where currents are unknown.

The main contribution of this work is the implementation of a range-based navigation system in geodetic coordinates for an AUV. This range-based navigation system is implemented in the World Geodetic System 1984 (WGS 84) coordinate reference system. The navigation system is not restricted to the WGS 84 ellipsoid and can be applied to any reference ellipsoid. This thesis documents the formulation of the navigation system in geodetic coordinates. Experimental data gathered in Claytor Lake, VA, and the Chesapeake Bay is presented.

Range-Based Autonomous Underwater Vehicle Navigation Expressed in Geodetic Coordinates

Rami S. Jabari

(GENERAL AUDIENCE ABSTRACT)

Unlike many terrestrial applications, GPS is unavailable to autonomous underwater vehicles (AUVs) while submerged due to the rapid attenuation of radio frequency signals in seawater. Underwater vehicles often use other navigation technologies. This thesis describes a range-based acoustic navigation system that utilizes range, or distance, measurements from a single moving beacon with a known location to estimate the position of an AUV in geodetic coordinates (latitude and longitude). Additionally, the navigation system simultaneously estimates the ocean currents acting on the AUV. Thus the navigation system can be used in locations where currents are unknown.

The main contribution of this work is the implementation of a range-based navigation system in geodetic coordinates for an AUV. By using range-based navigation, an AUV can accurately estimate its position while submerged. This range-based navigation system is implemented in the World Geodetic System 1984 (WGS 84) coordinate reference system, which is commonly used to describe Earth's shape. The navigation system is not restricted to WGS 84. This thesis documents the formulation of the navigation system in geodetic coordinates. Experimental data gathered in Claytor Lake, VA, and the Chesapeake Bay is presented.

To My Father, Mother, and Jessica

Acknowledgments

There are many people whom I would like to thank for supporting me during my graduate school endeavors.

First and foremost, I would like to thank my advisor Dr. Daniel Stilwell. His assistance and guidance during my career as a graduate research assistant has been invaluable. Additionally, I am grateful to the other members on my thesis committee, Dr. Wayne Neu and Dr. Craig Woolsey, for their advice and help.

I would like to deeply thank my fellow labmates of the Autonomous Systems and Controls Lab (ASCL) at Virginia Tech. I truly enjoyed working with all of them over the years. We did great work together and shared some unforgettable laughs.

Finally, I am grateful for the support I received from my parents and Jessie. They provided me with the needed encouragement and support during my stay at Virginia Tech. I will be forever indebted to them.

Contents

Dedication	iv
Acknowledgments	v
1 Introduction	1
1.1 Contribution	2
1.2 Motivation	2
1.3 Related Work	4
1.4 Organization	6
2 Preliminaries	7
2.1 Introduction	7
2.2 Notation	7
2.3 Background	8
2.3.1 Coordinate Systems	9
2.3.2 Haversine Formula	14
2.3.3 Kinematic Model in Cartesian Coordinates	15
2.4 The Extended Kalman Filter	16
3 Range Navigation System	19
3.1 Basics of Acoustic Ranging	19
3.1.1 Practical Issues	21
3.2 Algorithm Formulation	22
3.2.1 Kinematic Model	24

3.2.2	Observation Model	26
3.2.3	Rejection of Inaccurate Range Measurements	27
3.3	The Extended Kalman Filter for Range Navigation	29
4	Experimental Results and Performance Assessment	32
4.1	Experimental Apparatus	32
4.2	Assessment of Range Measurements and Their Performance	37
4.3	Assessment of Navigation Performance Without Currents in Claytor Lake . .	39
4.4	Assessment of Navigation Performance with Currents in the Chesapeake Bay	47
4.4.1	Experimental Setup Modifications	48
4.4.2	Assessment of Position Estimation	49
4.4.3	Assessment of Current Estimation	54
5	Conclusions	58
	Appendix A Destination Latitude and Longitude	64
	Appendix B Jacobians	68

List of Figures

2.1	Lines of Latitude and Longitude	10
2.2	ECEF Frame	11
2.3	NED Frame	12
2.4	AUV Coordinate Frame	14
3.1	AUV to Shore Acoustic Communication	20
4.1	The Virginia Tech 690s AUV	33
4.2	Teledyne Benthos Acoustic Modem and Transducer Combination	35
4.3	Teledyne Benthos Universal Deck Box	36
4.4	Shore Transducer	37
4.5	Claytor Lake	38
4.6	Claytor Lake Mission 1	41
4.7	Range Measurements from Claytor Lake Mission 1	42
4.8	Claytor Lake Mission 2	42
4.9	Range Measurements from Claytor Lake Mission 2	43
4.10	Claytor Lake Mission 3	43
4.11	Range Measurements from Claytor Lake Mission 3	44
4.12	Claytor Lake Mission 4	44
4.13	Range Measurements from Claytor Lake Mission 4	45
4.14	Claytor Lake Local NED vs Geodetic Range Navigation Solution	46
4.15	Chesapeake Bay Operation Area	47

4.16 Fixed Shore Transducer Mount	48
4.17 Chesapeake Bay Mission CB1	51
4.18 Range Measurements from Chesapeake Bay Mission CB1	51
4.19 Chesapeake Bay Mission CB2	52
4.20 Range Measurements from Chesapeake Bay Mission CB2	52
4.21 Chesapeake Bay Local NED vs Geodetic Range Navigation Solution	54
4.22 Geodetic Current Estimation for CB1	55
4.23 Geodetic Current Estimation in the Chesapeake Bay in m/s for CB1	56
4.24 Geodetic Current Estimation for CB2	56
4.25 Geodetic Current Estimation in the Chesapeake Bay in m/s for CB2	57
A.1 Destination Latitude and Longitude from Initial Latitude and Longitude	65

List of Tables

1.1	Advantages and Disadvantages of Range Navigation	3
2.1	World Geodetic System 1984 (WGS 84) Parameters	9
4.1	The Virginia Tech 690s AUV Specifications	33
4.2	The Virginia Tech 690s Sensor Suite	34
4.3	Claytor Lake Mission Descriptions	40
4.4	Distance Errors from Claytor Lake Trials	45
4.5	Chesapeake Bay Mission Descriptions	50
4.6	Distance Errors from Chesapeake Bay Trials	53

List of Acronyms

AHRS attitude and heading reference system

AUV autonomous underwater vehicle

DVL Doppler Velocity Log

ECEF Earth-Centered Earth-Fixed

EKF extended Kalman filter

FOG fiber optic gyroscope

GPS Global Positioning System

IMU inertial measurement unit

LBL long baseline

LLA latitude-longitude-altitude

NED North East Down

RF radio frequency

RPM revolutions per minute

6DoF six degrees of freedom

ToA time of arrival

UDB Universal Deck Box

WGS 84 World Geodetic System 1984

Nomenclature

h altitude

α angle of attack

ΔT change in time

\mathbf{P} EKF error covariance

\mathbf{K} EKF Kalman gain

ν EKF measurement noise

\mathbf{R} EKF measurement noise covariance

ω EKF process noise

\mathbf{Q} EKF process noise covariance

\mathbf{F} EKF state transition matrix

f EKF kinematic (state transition) model

\mathbf{x} EKF state vector

\mathbf{H} EKF measurement matrix

h EKF measurement model

\mathbf{z} EKF measurement vector

\mathbb{E} expectation

f flattening

φ latitude

λ longitude

θ pitch
 q pitch rate
 ϕ roll
 p roll rate
 a semi-major axis
 $\mathbb{Z}_{\geq 0}$ set of non-negative integers
 β sideslip angle
 c speed of sound
 \mathbb{R}^3 three-dimensional real space
 T transpose
 \mathbb{R}^2 two-dimensional real space
 \mathbf{V} velocity
 \mathbf{X}_{ECEF} \mathbf{X} -axis in the ECEF coordinate frame
 \mathbf{X}_{NED} \mathbf{X} -axis in the NED coordinate frame
 x_b x -axis in the AUV body frame
 u x -axis AUV body velocity (surge)
 \mathbf{Y}_{ECEF} \mathbf{Y} -axis in the ECEF coordinate frame
 \mathbf{Y}_{NED} \mathbf{Y} -axis in the NED coordinate frame
 y_b y -axis in the AUV body frame
 v y -axis AUV body velocity (sway)
 ψ yaw
 r yaw rate
 \mathbf{Z}_{ECEF} \mathbf{Z} -axis in the ECEF coordinate frame
 \mathbf{Z}_{NED} \mathbf{Z} -axis in the NED coordinate frame
 z_b z -axis in the AUV body frame
 w z -axis AUV body velocity (heave)

Chapter 1

Introduction

Due to the rapid attenuation of radio frequency (RF) signals in water, Global Positioning System (GPS) is not available to underwater vehicles. Autonomous underwater vehicles (AUVs) utilize other forms of navigation technologies while submerged. This work proposes a range-based acoustic navigation system for AUVs. The range-based navigation system, which takes into account geodetics, is implemented in the World Geodetic System 1984 (WGS 84) coordinate reference system.

A geodetic coordinate system is used to express the location of a point on Earth. Geodetic coordinates are commonly expressed as latitude-longitude-altitude (LLA). In many applications, the geodetic reference system is defined as an ellipsoid. The reference ellipsoid is defined by a semi-major axis and a flattening coefficient. This work uses the WGS 84 ellipsoid defined in Subsection [2.3.1](#). The proposed range navigation system is not restricted to the WGS 84 ellipsoid and can be applied to any reference ellipsoid.

Range (or distance) measurements are acquired from a moving acoustic transponder with a known location. The navigation system estimates the position of an AUV by using measurements of the AUV's heading and speed (or velocity), range measurements, and an initial

estimate of the AUV's position prior to diving. The navigation system can simultaneously estimate currents and the AUV's location.

1.1 Contribution

The main contribution of this work is the implementation of a range-based navigation system in geodetic coordinates for an AUV. The proposed navigation algorithm has been implemented on the Virginia Tech 690s AUV, which uses an acoustic modem and transducer to acquire range measurements from an external acoustic transponder that is mounted to a moving boat with a known location. Successful experimental testing was conducted in the Chesapeake Bay and in Claytor Lake, VA.

This work is not limited to using a single acoustic transponder. Additionally, this navigation system can be modified to use another AUV with an acoustic modem and a known location instead of a boat.

1.2 Motivation

Two commonly used forms of technology for underwater navigation are inertial and acoustic navigation systems. Range-based navigation is a type of acoustic navigation: an AUV acquires range (or distance) measurements between itself and a possibly moving beacon whose location is known. Range is computed via the round-trip time-of-flight of an acoustic signal. By utilizing additional measurements of the vehicle's heading and speed, depth, and a rough estimate of the initial AUV position, a range navigation system can estimate a vehicle's position. In this thesis, an extended Kalman filter (EKF) is used to compute the position estimate.

Volume, cost constraints, and complexity play a large factor in determining what navigation system will be used on an AUV. Sensors like a highly calibrated inertial measurement unit (IMU), fiber optic gyroscope (FOG), or Doppler Velocity Log (DVL) are costly and/or bulky. Additionally, long baseline (LBL) acoustic navigation systems have a complex setup due to the requirements that transponders be deployed and surveyed on the seafloor. As stated in [1], range navigation is beneficial to small, low-cost AUVs because it provides a low-power, low-cost, low-volume, and low-complexity alternative to other underwater navigation algorithms. Table 1.1 describes the advantages and disadvantages of a range-based navigation system.

Table 1.1: Advantages and Disadvantages of Range Navigation

Advantages	Disadvantages
Range measurements can be acquired easily if acoustic communication is available	Requires the ability to communicate acoustically
Reference beacon (e.g., boat or buoy) does not need to be pre-deployed into the seafloor and pre-surveying is not needed	Must always know the location of the reference beacon
Location of reference beacon does not need to be fixed	Not useful for a vehicle running solo missions since a reference beacon is needed
Only one reference beacon is required while LBL needs multiple fixed reference beacons	Requires an environment that does not interfere with acoustic signals
Range navigation solution does not drift like inertial navigation does over an extended period of time	Not suitable for stealth missions

GPS receivers obtain data in LLA coordinates. However, many navigation solutions utilize transformations from LLA to a local coordinate frame. The use of local coordinates requires some amount of bookkeeping. A local coordinate system is only accurate for a limited distance and then a new local frame needs to be selected. As technology advances, AUVs will be able to traverse longer distances and complete longer missions, resulting in

more bookkeeping. The proposed geodetic range navigation algorithm does not use transformations from a global coordinate frame to local frames or vice versa. For this work, no computations are completed in a local frame and the bookkeeping that can arise when using a local coordinate system is avoided.

1.3 Related Work

There has been a large amount of research conducted in underwater navigation systems for AUVs, with the two most common classes of navigation approaches being inertial and acoustic navigation. Range-based navigation falls under the acoustic class of navigation systems. The typical example of an acoustic navigation system is long baseline (LBL), which uses an array of transponders on the seafloor to determine the position of an underwater vehicle. Recently in [2] an LBL localization system was developed for an underwater glider. The LBL system in [2] utilizes the Rauch-Tung-Striebel smoothing algorithm to improve an EKF's position estimate.

Previous research conducted in the area of range navigation via measurements from a single beacon exists. Gadre contributed an observability analysis in [1], [3], [4], and [5]. It is shown that most trajectories of the range-based navigation system are locally observable, except for straight-line trajectories whose extensions pass through the location of the transponder. Local observability in this case implies that an observer such as an EKF can estimate the position of the AUV so long as the initial condition is sufficiently accurate. In Gadre's work, the AUV's velocity is estimated via a heading measurement from an attitude and heading reference system (AHRS) and speed that is estimated via a mapping from the propeller's angular rate measured in revolutions per minute (RPM) to the AUV's surge velocity expressed in m/s. The observability analysis is extended in [6] to incorporate depth. Later work [7] shows the advancements of range navigation by using more sophisti-

cated sensors such as a DVL for velocity estimates. A centralized extended Kalman filter is implemented in [7] to estimate vehicle position for deep-water surveying and it is shown that utilizing range measurements from a single beacon for subsea navigation is a suitable alternative to LBL.

The range-based navigation concept is still being researched and expanded upon by a few. Most recently, in [8], an approach is proposed to simultaneously localize an AUV and multiple beacons. Cooperative navigation is a major extension of acoustic ranging from a single beacon. Researchers report in [9] a preliminary study, which utilizes range-rate in addition to range, for a cooperative navigation algorithm using one underwater vehicle and one surface vehicle. Only a few have reported studies that utilize range-rate in addition to range. Based on preliminary results in [9], it is explained that the addition of range-rate may not have a significant impact on performance of a centralized extended Kalman filter. Cooperative path planning algorithms are proposed in [10] and a beacon vehicle supports multiple survey vehicles. The path of the beacon vehicle is planned to keep survey vehicle position errors low. An algorithm designed to position beacon vehicles in locations that minimize survey vehicle position errors is presented in [11]. It should be noted that all of this previous research is done in a local coordinate frame.

Acoustic navigation is not limited to the use of acoustic beacons. Two-dimensional sonar imagery is used to aid underwater navigation systems in [12], [13], and [14]. In [12], an AUV with a forward-looking sonar navigates relative to features that appear in a sonar image given an *a priori* map of the features. Similar to [12], researchers in [13] and [14] incorporate simultaneous localization and mapping (SLAM) algorithms that utilize a forward-looking sonar.

1.4 Organization

Chapter 2 covers the notation used and preliminaries needed to implement a range navigation algorithm on an AUV using the WGS 84 coordinate reference system. The formulation of the range navigation algorithm in geodetic coordinates is shown in Chapter 3. Chapter 4 elaborates on the hardware used. Additionally, data collection and algorithm results are analyzed in Chapter 4. The thesis is concluded in Chapter 5.

Chapter 2

Preliminaries

2.1 Introduction

This chapter elaborates on the preliminaries needed to understand and implement a range navigation system. Notation is introduced in this chapter, along with the background required to grasp different coordinate frames, general AUV kinematics, dead reckoning, and the extended Kalman filter (EKF).

2.2 Notation

Standard notation is used in this thesis. Bold uppercase letters represent matrices while bold lowercase letters represent vectors. Discrete time index k is in the set of non-negative integers $\mathbb{Z}_{\geq 0}$. The two-dimensional and three-dimensional real spaces are denoted as \mathbb{R}^2 and \mathbb{R}^3 , respectively. The unit sphere is denoted as \mathcal{S}^2 . All other notation is defined before it is used.

2.3 Background

The proposed geodetic range navigation algorithm estimates the position of an AUV in the World Geodetic System 1984 (WGS 84) coordinate reference frame. The WGS 84 geodetic datum is an ellipsoid and is explicitly defined in Subsection 2.3.1. To model the motion of an AUV with respect to the reference ellipsoid, a kinematic model of the AUV using geodetic coordinates is derived in Chapter 3. In previous work ([1], [3], [4], [5]), a local Cartesian coordinate frame is used for range navigation. The local range navigation system is a North East Down (NED) coordinate system where the \mathbf{X}_{NED} -axis points due North, the \mathbf{Y}_{NED} -axis points due East, and the \mathbf{Z}_{NED} -axis points towards the center of the Earth. The origin of the NED frame is fixed to an arbitrary point on Earth's surface. The location of a point in the NED frame can be denoted as $(x_{NED}, y_{NED}, z_{NED})$. A more detailed description of the NED frame is in Subsection 2.3.1. The local range navigation system estimates local x_{NED} and y_{NED} positions along with currents in the x_{NED} and y_{NED} directions. Depth, or the z_{NED} position, is measured via a pressure sensor.

The proposed range navigation solution, in geodetic coordinates, is compared against the range navigation solution from [1], which is in a local coordinate frame. The geodetic range navigation solution is additionally compared to a geodetic dead reckoning solution. Subsection 2.3.1 further elaborates on WGS 84 and other coordinate systems. Subsection 2.3.2 outlines how to calculate the shortest distance between two points of interest and Subsection 2.3.3 describes the kinematic model.

2.3.1 Coordinate Systems

World Geodetic System 1984

The World Geodetic System 1984 (WGS 84) [15] is a geodetic coordinate system that is used in many GPS based navigation systems. The WGS 84 ellipsoid is defined by two main parameters a and f , which are the semi-major axis and flattening, respectively. With these two defining parameters, geometric constants are derived to represent the geometry of the WGS 84 ellipsoid. The derived constants include, but are not limited to, the semi-minor axis, eccentricity, and radius of curvature. If a geodetic datum other than the WGS 84 ellipsoid is used, the constants are different. Table 2.1 shows the constants that are used throughout this thesis.

Table 2.1: WGS 84 Parameters

Symbol	Description	Value
a	Semi-major axis	6378137.0 m
b	Semi-minor axis	6356752.3142 m
e^2	First eccentricity squared	$6.69437999014 \times 10^{-3}$
$\frac{1}{f}$	Inverse flattening	298.257223563

A location relative to the WGS 84 ellipsoid is expressed in terms of latitude, longitude, and altitude. Latitude φ is the angular distance from the Earth's equator, where a measurement north of the equator is positive and a measurement south of the equator is negative. Longitude λ is the angular distance from the Earth's prime meridian, where a measurement east of the prime meridian is positive and a measurement west of the prime meridian is negative. Lines of latitude range from -90° to 90° while lines of longitude range from -180° to 180° . Altitude h is the distance along the ellipsoidal normal. Positive altitude points away from the ellipsoid's interior. The location of a point relative to the WGS 84 ellipsoid is denoted as $\mathbf{g} = (\varphi, \lambda, h)$ in $\mathcal{S}^2 \times \mathbb{R}$. Figure 2.1 illustrates the lines of latitude and longitude on the WGS 84 ellipsoid.

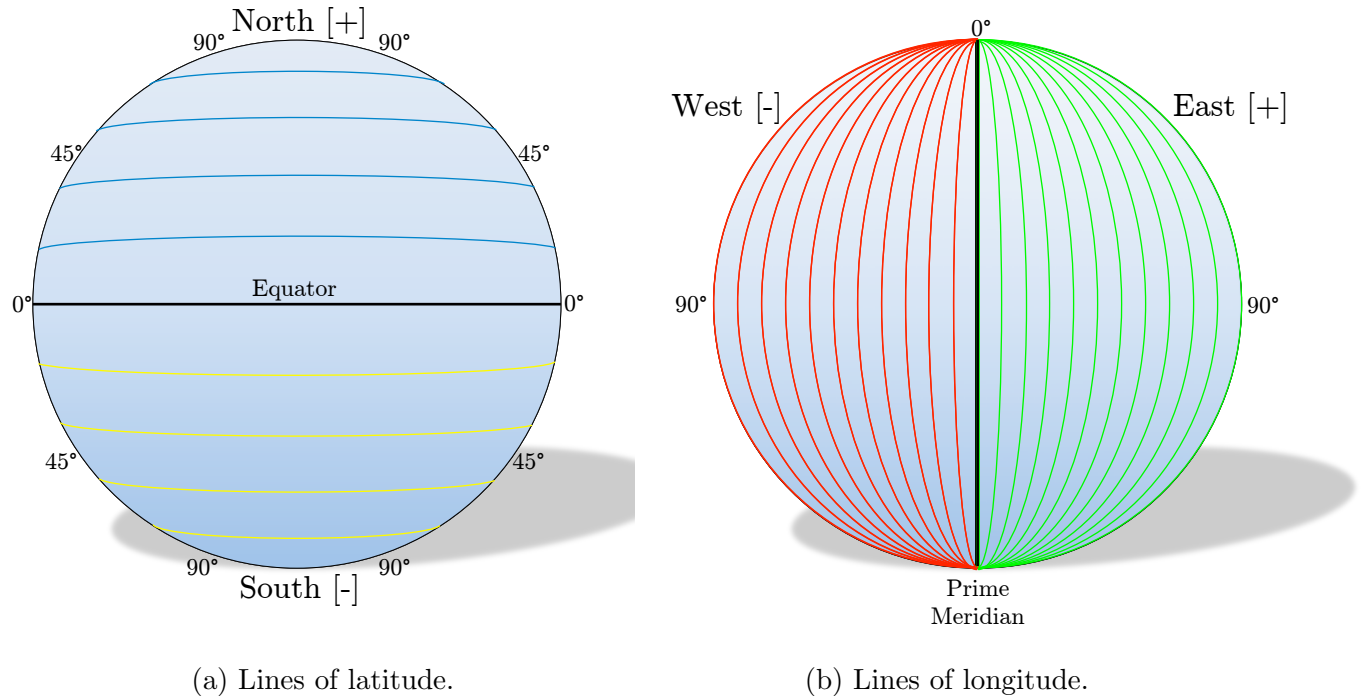


Figure 2.1: Lines of latitude, in units of degrees, are illustrated in 2.1a. Lines of longitude, in units of degrees, are illustrated in 2.1b. Due to figure complexity and not being able to illustrate lines on the backside of the sphere, lines of longitude are illustrated from -90° to 90° .

Earth-Centered Earth-Fixed

The Earth-Centered Earth-Fixed (ECEF) coordinate frame, described in [16], is a Cartesian coordinate system and has its origin fixed at the center of the Earth. The ECEF coordinate system is illustrated in Figure 2.2. The ECEF coordinate frame has the axes \mathbf{X}_{ECEF} , \mathbf{Y}_{ECEF} , \mathbf{Z}_{ECEF} . The axis \mathbf{X}_{ECEF} extends through the intersection of the prime meridian and the equator (0° , 0°). The axis \mathbf{Y}_{ECEF} extends through the intersection of the equator and 90° longitude (0° , 90°). The axis \mathbf{Z}_{ECEF} completes the right-handed coordinate system and extends through the true north pole (90° , 0°). The location of a point in the ECEF frame is denoted as $(x_{ECEF}, y_{ECEF}, z_{ECEF})$.

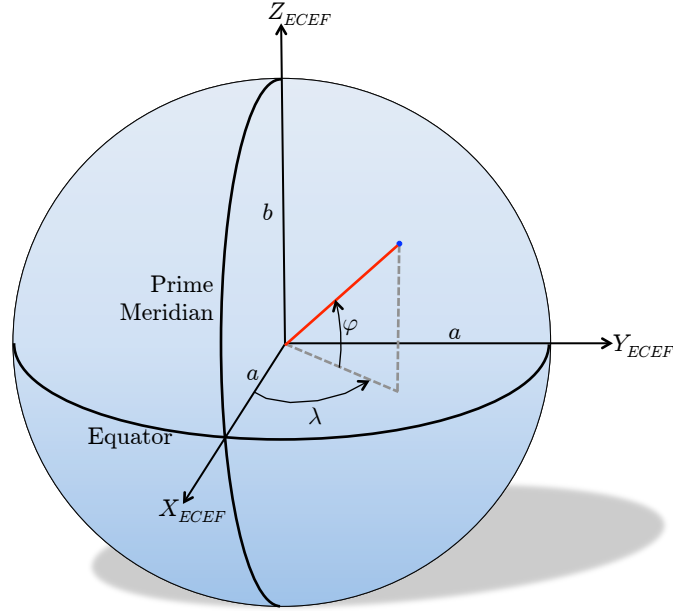


Figure 2.2: The ECEF coordinate frame is illustrated above and has the axes \mathbf{X}_{ECEF} , \mathbf{Y}_{ECEF} , \mathbf{Z}_{ECEF} . a and b are the semi-major and semi-minor axes, respectively. φ is latitude and λ is longitude.

Geodetic coordinates on the WGS 84 ellipsoid can be transformed from LLA to rectangular ECEF coordinates via the closed form formulas

$$x_{ECEF} = (N(\varphi) + h) \cos \varphi \cos \lambda \quad (2.1a)$$

$$y_{ECEF} = (N(\varphi) + h) \cos \varphi \sin \lambda \quad (2.1b)$$

$$z_{ECEF} = [(1 - e^2) N(\varphi) + h] \sin \varphi \quad (2.1c)$$

The altitude h is the distance along the ellipsoidal normal, between the ellipsoid's surface and the point of interest. The radius of curvature in the prime vertical $N(\varphi)$ is defined as

$$N(\varphi) = \frac{a}{\sqrt{1 - e^2 \sin^2 \varphi}} \quad (2.2)$$

North East Down

A North East Down (NED) frame is a local coordinate system that is fixed to Earth's surface. The origin is a fixed location on Earth's surface and is arbitrarily chosen. Following the convention of a right-handed coordinate system, the \mathbf{X}_{NED} -axis and \mathbf{Y}_{NED} -axis point toward the WGS 84 ellipsoid north (geodetic or true north) and east (geodetic east), respectively. The \mathbf{Z}_{NED} -axis points downward toward the center of the Earth, normal to the ellipsoid. The location of a point in the NED frame can be denoted as $(x_{NED}, y_{NED}, z_{NED})$. Figure 2.3 shows the NED local coordinate system.

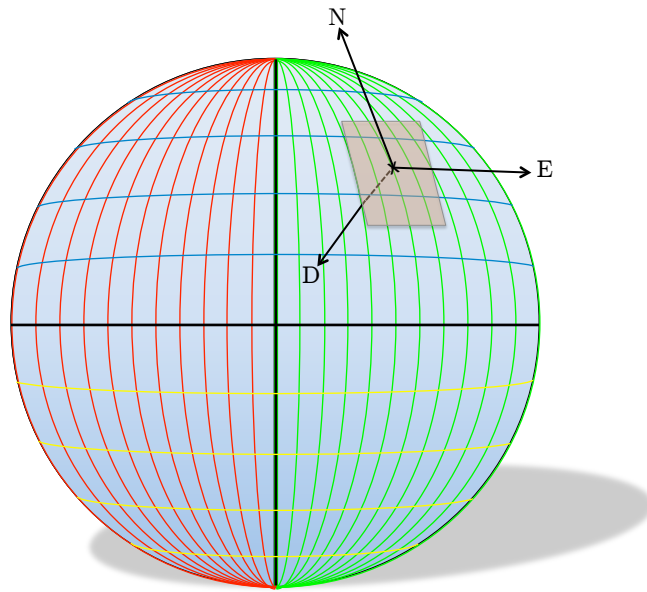


Figure 2.3: The NED coordinate system is shown above. The \mathbf{X}_{NED} axis is pointed north, the \mathbf{Y}_{NED} axis is pointed east, and the \mathbf{Z}_{NED} axis is pointed down toward Earth's center.

AUV or Body Frame

The terminology used in this section is standard and follows [17]. The notation differs slightly from that in [17]. The AUV frame is based on the motion of a rigid body that has six degrees of freedom (6DoF). Figure 2.4 illustrates the AUV frame. The body-fixed axes are denoted as x_b , y_b , z_b . The x_b -axis is defined in the forward direction of the vehicle. The y_b -axis is defined pointing to the right of the vehicle. The z_b -axis is defined pointing through the bottom of the vehicle and completes the right-handed coordinate system. The motion of the AUV frame is described relative to an Earth-fixed reference frame such as NED. The orientation of the AUV with respect to the Earth-fixed frame is described by the Euler angles roll ϕ , pitch θ , and yaw ψ . The yaw measured in the AUV frame is the same as the yaw measured in the NED frame. Body angular rates about the x_b , y_b , and z_b axes are p , q , and r , respectively. Body velocities along the x_b , y_b , and z_b axes are denoted as u , v , and w , respectively. The vehicle's velocity is denoted as $\mathbf{V} = [u, v, w]$. The angle between the projection of \mathbf{V} onto the x_b - y_b plane and the x_b -axis is the sideslip angle, β . The angle between the projection of \mathbf{V} onto the x_b - z_b plane and the x_b -axis is the angle of attack, α .

For this thesis, the roll, pitch, and yaw angles are measured via an AHRS that is on the vehicle. The yaw, or heading, is measured in degrees clockwise from north. It is important to note that the heading measurement is relative to magnetic north and not true (geodetic) north; hence, it is important to factor in the magnetic declination in the area of operation.

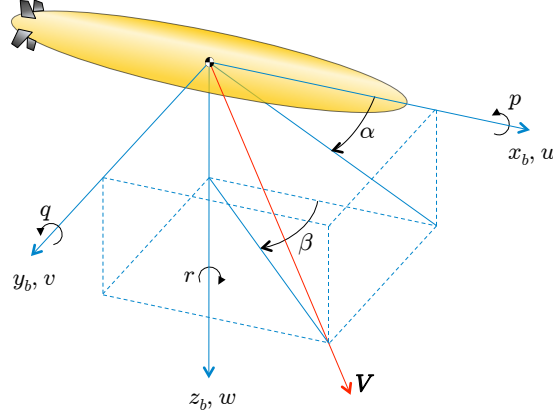


Figure 2.4: The AUV, or body, frame is illustrated above with body axes x_b , y_b , and z_b .

2.3.2 Haversine Formula

The Haversine formula [18] was developed to calculate the great-circle distance d_h between two points on the surface of a sphere given their latitude and longitude. The great-circle distance is the shortest distance measured between two points along a sphere's surface.

The great-circle distance between $\mathbf{g}_1 = [\varphi_1, \lambda_1]$ and $\mathbf{g}_2 = [\varphi_2, \lambda_2]$ is computed using the Haversine formula in (2.3). The latitude and longitude coordinates are expressed in radians. The variable ϵ is the square of half the chord length between \mathbf{g}_1 and \mathbf{g}_2 , γ is the angular distance in radians, and R is the radius of the sphere. The units of d_h depends on the units of R . If R is in meters, then d_h is in meters.

$$\epsilon = \sin^2 \left(\frac{\varphi_2 - \varphi_1}{2} \right) + \cos(\varphi_1) \cos(\varphi_2) \sin^2 \left(\frac{\lambda_2 - \lambda_1}{2} \right) \quad (2.3a)$$

$$\gamma = 2 \cdot \text{atan2} \left(\sqrt{\epsilon}, \sqrt{1 - \epsilon} \right) \quad (2.3b)$$

$$d_h = R\gamma \quad (2.3c)$$

Since the Haversine formula incorporates a sphere's radius, distance calculations between two points on the surface are more accurate over longer distances than a two-dimensional Euclidean distance, which has no curvature.

2.3.3 Kinematic Model in Cartesian Coordinates

This section describes the development of an AUV kinematic model. By utilizing information regarding speed, change in time, and heading, the current position can be estimated based on the location at the previous time step. Denote the change in time, between time steps k and $k - 1$, as ΔT . By knowing the speed $u[k - 1]$, heading $\psi[k - 1]$, and previous location, the location estimate at time k in a local Cartesian coordinate frame is

$$x[k] = x[k - 1] + \Delta T u[k - 1] \cos(\psi[k - 1]) + \Delta T v_x \quad (2.4a)$$

$$y[k] = y[k - 1] + \Delta T u[k - 1] \sin(\psi[k - 1]) + \Delta T v_y \quad (2.4b)$$

where v_x and v_y are the currents in the x and y directions.

Since a kinematic model is being used, it is assumed that there is no sideslip and the heading of the vehicle is the same as the direction it is moving in. In other words, it is assumed that v and w are 0.

This same process can be extended to geodetic coordinates. Assume that $(\varphi[k], \lambda[k])$ are the coordinates of the AUV at time k and $(\varphi[k - 1], \lambda[k - 1])$ are the coordinates of the AUV at the previous time step. If the initial heading at time $k - 1$, distance traveled along the great-circle, the radius of the sphere, and the position at time $k - 1$ are known, then an estimate of the AUV location at time k is

$$\varphi[k] = \sin^{-1}(\cos(\xi[u[k]]) \sin(\varphi[k - 1]) + \cos(\varphi[k - 1]) \cos(\psi[k - 1]) \sin(\xi[u[k]])) \quad (2.5a)$$

$$\lambda[k] = \lambda[k-1] + \operatorname{atan2}(\cos(\varphi[k-1]) \sin(\psi[k-1]) \sin(\xi[u[k]]), \cos(\xi[u[k]]) - \sin(\varphi[k]) \sin(\varphi[k-1])) \quad (2.5b)$$

where $\xi[u[k]] = \frac{\Delta T u[k-1]}{R}$ is the angular distance traveled and R is the radius of the Earth. All of the angles in (2.5) are in units of radians. If the distance traveled between two points is short, it is assumed that the change in heading is negligible for the great-circle route. This concept is further elaborated in Chapter 3. The National Oceanic and Atmospheric Administration (NOAA) [19] references Williams' 'Aviation Formulary' [20] for information on great-circle navigation, which contains (2.5). The function 'destPoint' from the geosphere package [21] is the equivalent of (2.5). Veness provides a useful summary of calculations using latitude and longitude points in [22]. A derivation of (2.5) is in Appendix A.

2.4 The Extended Kalman Filter

The extended Kalman filter (EKF) is a standard observer that is used often in navigation systems. A thorough derivation of both the Kalman filter and EKF can be found in [23]. The notation used in this thesis slightly differs from that in [23], but is the same conceptually.

A presumed kinematic model can be expressed as

$$\mathbf{x}[k] = \mathbf{f}(\mathbf{x}[k-1], k) + \boldsymbol{\omega}[k] \quad (2.6)$$

$$\mathbf{z}[k] = \mathbf{h}(\mathbf{x}[k]) + \boldsymbol{\nu}[k] \quad (2.7)$$

where $\mathbf{x}[k]$ is the state vector and $\mathbf{z}[k]$ is the measurement vector. The noise models, $\boldsymbol{\omega}$ and $\boldsymbol{\nu}$, are zero-mean multivariate normal distributions with covariances \mathbf{Q} and \mathbf{R} for process and measurement, respectively.

The prediction of the system state (2.6) at time k given the information available at time $k - 1$ is $\mathbf{x}[k|k - 1]$. The estimate of the system state at time k given information available up to time k is $\mathbf{x}[k|k]$. Prediction of the system state and state estimation error covariance are expressed as

$$\mathbf{x}[k|k - 1] = \mathbf{f}(\mathbf{x}[k - 1], k) \quad (2.8a)$$

$$\mathbf{P}[k|k - 1] = \mathbf{F}[k]\mathbf{P}[k - 1|k - 1]\mathbf{F}[k]^\top + \mathbf{Q}[k] \quad (2.8b)$$

where \mathbf{P} is the estimation error covariance that is propagated along with the state estimate.

Given a measurement $\mathbf{z}[k]$, the state estimate and estimation error covariance are expressed as

$$\mathbf{K}[k] = \mathbf{P}[k|k - 1]\mathbf{H}[k]^\top(\mathbf{H}[k]\mathbf{P}[k|k - 1]\mathbf{H}[k]^\top + \mathbf{R}[k])^{-1} \quad (2.9a)$$

$$\mathbf{x}[k|k] = \mathbf{x}[k|k - 1] + \mathbf{K}[k](\mathbf{z}[k] - \mathbf{h}(\mathbf{x}[k])) \quad (2.9b)$$

$$\mathbf{P}[k|k] = (\mathbf{I} - \mathbf{K}[k]\mathbf{H}[k])\mathbf{P}[k|k - 1] \quad (2.9c)$$

where \mathbf{K} is the Kalman gain. The state transition matrix \mathbf{F} and observation matrix \mathbf{H} are the Jacobians

$$\mathbf{F}[k - 1] = \left. \frac{\partial \mathbf{f}}{\partial \mathbf{x}} \right|_{\mathbf{x}[k-1]|\mathbf{x}[k-1]} \quad (2.10a)$$

$$\mathbf{H}[k] = \left. \frac{\partial \mathbf{h}}{\partial \mathbf{x}} \right|_{\mathbf{x}[k]|\mathbf{x}[k-1]} \quad (2.10b)$$

The state \mathbf{x} and the error covariance \mathbf{P} are initialized

$$\mathbf{x}[0|0] = \mathbb{E}[\mathbf{x}[0]] \quad (2.11a)$$

$$\mathbf{P}[0|0] = \mathbb{E}[(\mathbf{x}[0] - \mathbb{E}[\mathbf{x}[0]])(\mathbf{x}[0] - \mathbb{E}[\mathbf{x}[0]])^\top] \quad (2.11b)$$

where \mathbb{E} is the expectation operator. \mathbf{Q} and \mathbf{R} should be selected based on how accurate the model and measurements are, respectively.

Chapter 3

Range Navigation System

This chapter describes the concept of acoustic ranging, describes practical issues, formulates the range-based navigation algorithm, proposes a way to reject inaccurate range measurements, and formulates the EKF for the proposed range navigation algorithm.

3.1 Basics of Acoustic Ranging

The concept of acoustic ranging is based on the time of arrival (ToA) of acoustic signals between transducers. For the scenario in this thesis, an acoustic modem and transducer combination on an AUV pings a remote acoustic modem and transducer, which can be on a boat, another AUV, a buoy, etc. A return signal is sent and a range measurement is calculated via the round-trip time-of-flight of the acoustic signal. The return signal from the remote modem contains encoded information, such as the remote modem's GPS coordinates and depth, in its data packet. Figure 3.1 illustrates an AUV pinging a transducer that is fixed to the side of a boat. For this thesis, the remote modem is referred to as the shore modem and the remote transducer is referred to as the shore transducer. The shore modem

and transducer are fixed to a boat.

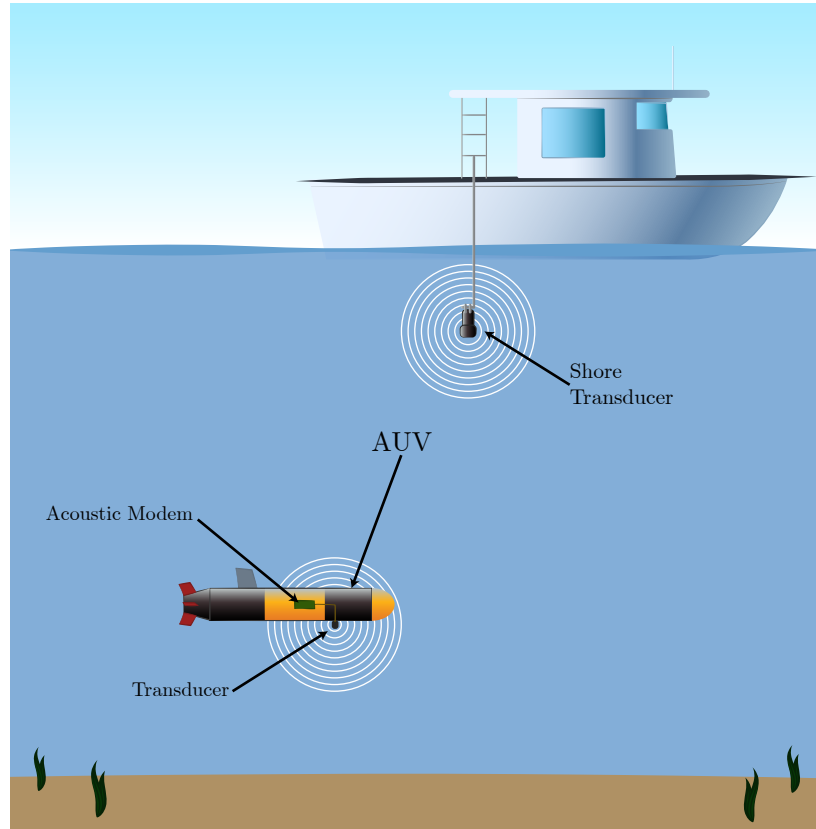


Figure 3.1: The AUV is shown pinging the shore modem and transducer combination that is fixed to a boat.

For the range measurements to be accurate, it is assumed that the speed of sound c in the operation medium is known. The speed of sound in water can be approximated if the depth, temperature, and salinity are known. One approach to calculate the speed of sound in ocean water is the Mackenzie Equation [24]

$$\begin{aligned}
 c(\delta, \Upsilon, \tau) = & 1448.96 + 4.591\tau - 5.304 \times 10^{-2}\tau^2 + 2.374 \times 10^{-4}\tau^3 + 1.340(\Upsilon - 35) \\
 & + 1.630 \times 10^{-2}\delta + 1.675 \times 10^{-7}\delta^2 - 1.025 \times 10^{-2}\tau(\Upsilon - 35) \\
 & - 7.139 \times 10^{-13}\tau\delta^3
 \end{aligned} \tag{3.1}$$

where δ is the depth in meters, Υ is the salinity in parts per thousand, and τ is the water temperature in degrees Celsius. The Mackenzie Equation is only valid for temperatures ranging from -2 to 30 degrees Celsius, salinity 30 to 40 parts per thousand, and depth 0 to 8000 meters.

For water with a lower salinity content, an alternative is Coppens' Equation [25]

$$c(\delta, \Upsilon, \tau') = c(0, \Upsilon, \tau') + (16.23 + 0.253\tau')\delta + (0.213 - 0.1\tau')\delta^2 + [0.016 + 0.0002(\Upsilon - 35)](\Upsilon - 35)\tau'\delta \quad (3.2a)$$

$$c(0, \Upsilon, \tau') = 1449.05 + 45.7\tau' - 5.21\tau'^2 + 0.23\tau'^3 + (1.333 - 0.126\tau' + 0.009\tau'^2)(\Upsilon - 35) \quad (3.2b)$$

where δ is the depth in kilometers, Υ is the salinity in parts per thousand, and τ' is $\frac{\tau}{10}$ where τ the water temperature in degrees Celsius. Coppens' Equation is only valid for temperatures ranging from 0 to 35 degrees Celsius, salinity 0 to 45 parts per thousand, and depth 0 to 4 kilometers.

3.1.1 Practical Issues

There are several practical issues that arise with underwater acoustic ranging. Errors in range measurements can arise from the assumed speed of sound in water being inaccurate. To approximate the speed of sound, (3.1) or (3.2) can be used. It is not uncommon to drop data packets due to multipath or signal fading. Multipath can be extreme in shallow water due to reflections from the water's surface and the sea floor. Another common source of multipath includes reflections from objects near the acoustic modem. Signal fading and attenuation can be a result of destructive interference due to multipath and sound absorption in water. Researchers in [26] discuss some of these issues along with the advancements in

acoustic communication. As mentioned in [27], other sources of interference include bubble plumes and propeller wakes. Small errors are present due to the vehicle moving between the time it pings a beacon and the time a measurement is received. There are instances when the encoded data sent with a range measurement (e.g., coordinates of the reference beacon) is incomplete or corrupted. Occasionally, a range measurement will be inaccurate. If an inaccurate measurement is not rejected, it can result in poor algorithm performance. A probabilistic approach to reject inaccurate range measurements is derived in Subsection 3.2.3.

3.2 Algorithm Formulation

In this section, it is shown that the results of the observability analysis conducted assuming local Cartesian coordinates are inherited by the range navigation problem expressed in geodetic coordinates. Additionally, this section documents the formulation of the state transition and measurement models used in the proposed geodetic range navigation system. The map from geodetic to ECEF coordinates in (2.1) can be modified to account for the vehicle depth δ

$$x_{ECEF} = (N(\varphi) + h - \delta) \cos \varphi \cos \lambda \quad (3.3a)$$

$$y_{ECEF} = (N(\varphi) + h - \delta) \cos \varphi \sin \lambda \quad (3.3b)$$

$$z_{ECEF} = [(1 - e^2) N(\varphi) + h - \delta] \sin \varphi \quad (3.3c)$$

For this chapter, x_{ECEF} , y_{ECEF} , and z_{ECEF} , incorporate a depth measurement, which is obtained from a pressure sensor on the vehicle. A detailed description of the sensors used on the AUV in this thesis can be found in Section 4.1. The altitude h is assumed to be constant in the operation area. Prior to conducting missions, the AUV acquires GPS data on the

surface of the water. The altitude is averaged and is assumed constant for that operation area.

Theorem 5.3.3 in [1] states straight line trajectories whose extension passes through the origin are not locally observable. The origin is the location of the reference beacon. In other words, the extension of an AUV straight-line trajectory that passes through the location of the shore transducer is not locally observable.

The linear time-varying (LTV) system

$$\begin{aligned}\dot{x}(t) &= A(t)x(t) \\ y(t) &= C(t)x(t)\end{aligned}\tag{3.4}$$

with initial condition $x(t_o) = x_o$ is *observable* on the interval $[t_o, t_1]$ if the initial condition can be uniquely determined by the output $y(t)$ for $t \in [t_o, t_1]$.

Suppose the nonlinear system

$$\begin{aligned}\dot{x}(t) &= f(x(t), t) \\ y(t) &= h(x(t), t)\end{aligned}\tag{3.5}$$

can be linearized about the trajectory $x_o(t)$, $t \in [t_o, t_1]$, yielding the LTV system (3.4). Then we say that the nonlinear system (3.5) is *locally observable* about the trajectory $x_o(t)$ if the corresponding LTV system (3.4) is observable on $[t_o, t_1]$.

We assume that $x(t) \in \mathbb{R}^3$ and that $y(t) \in \mathbb{R}$. Consider the function $\Psi : \mathbb{R}^3 \mapsto \mathcal{S}^2 \times \mathbb{R} \setminus \{(\varphi, \lambda, h) : \varphi = \pm \frac{\pi}{2}\}$ that maps Cartesian coordinates in an ECEF coordinate system to geodetic coordinates everywhere except the poles. Assume that the map Ψ is invertible,

differentiable, one-to-one, and onto. Let $s(t) = \Psi(x(t))$ and suppose that

$$\begin{aligned}\dot{s}(t) &= g(s(t), t) \\ y(t) &= h(\Psi^{-1}(s(t)), t)\end{aligned}\tag{3.6}$$

Note that the value of the output does not change under the proposed change of variables. Since Ψ is invertible, differentiable, one-to-one, and onto, the LTV system is locally observable in geodetic coordinates.

3.2.1 Kinematic Model

The kinematic model used for geodetic range navigation is derived in this section. The kinematic model \mathbf{f} is based on the geodetic kinematic model from Subsection 2.3.3 with the addition of currents. Denote the Euclidean distance between the two points \mathbf{p}_1 and \mathbf{p}_2 in \mathbb{R}^3 as

$$\begin{aligned}d(\mathbf{p}_1, \mathbf{p}_2) &= \|\mathbf{p}_1 - \mathbf{p}_2\| \\ &= \sqrt{(x_{ECEF,1} - x_{ECEF,2})^2 + (y_{ECEF,1} - y_{ECEF,2})^2 + (z_{ECEF,1} - z_{ECEF,2})^2}\end{aligned}\tag{3.7}$$

The AUV used in this work receives propeller rotation rate measurements from the motor controller connected to the propeller's motor, depth measurements from a pressure sensor, and heading measurements from an AHRS, at a rate of 10 Hz. Speed trials have been conducted to map RPM to AUV speed in meters per second. The distance traveled by the AUV is computed by multiplying the speed of the vehicle u in the x_b -axis with the timestep ΔT . It is assumed that there is no sideslip and the vehicle is traveling in the direction it is pointed.

Because ΔT is small, the simplifying assumption that the AUV travels on a sphere

with constant radius is made during each iteration of the kinematic model. The Earth is not a sphere so the radius is recomputed for every iteration of the kinematic model. This assumption is useful because it allows (2.5) to be used since a closed-form expression does not arise when it is assumed that the AUV moves strictly along the surface of an ellipsoid during ΔT .

The sphere's radius is the Euclidean distance from $\mathbf{p} = (x_{ECEF}, y_{ECEF}, z_{ECEF})$ to its center $\mathbf{0}$

$$\begin{aligned} d(\mathbf{p}, \mathbf{0}) &= \|\mathbf{p} - \mathbf{0}\| \\ &= \sqrt{x_{ECEF}^2 + y_{ECEF}^2 + z_{ECEF}^2} \end{aligned} \quad (3.8)$$

which can be rewritten in terms of $\mathbf{g} = (\varphi, \lambda, h)$

$$d_g(\mathbf{g}, \mathbf{0}) = \sqrt{(\mu \cos \varphi \cos \lambda)^2 + (\mu \cos \varphi \sin \lambda)^2 + (\rho \sin \varphi)^2} \quad (3.9)$$

where $\mu = (N(\varphi) + h - \delta)$ and $\rho = [(1 - e^2)N(\varphi) + h - \delta]$.

The kinematic model $\mathbf{f}(\mathbf{x}[k-1], k)$ expressed in geodetic coordinates is

$$\mathbf{f}(\mathbf{x}[k-1], k) = \begin{bmatrix} \varphi[k] \\ \lambda[k] \\ v_\varphi[k] \\ v_\lambda[k] \end{bmatrix} = \begin{bmatrix} \sin^{-1}(\Xi + \Sigma) \\ \lambda[k-1] + \text{atan2}(\chi, \Omega) \\ v_\varphi[k-1] \\ v_\lambda[k-1] \end{bmatrix} + \Delta T \begin{bmatrix} v_\varphi[k-1] \\ v_\lambda[k-1] \\ 0 \\ 0 \end{bmatrix} \quad (3.10)$$

where $\Xi = \cos(\xi[u[k]]) \sin(\varphi[k-1])$,

$$\Sigma = \cos(\varphi[k-1]) \cos(\psi[k-1]) \sin(\xi[u[k]]),$$

$$\chi = \cos(\varphi[k-1]) \sin(\psi[k-1]) \sin(\xi[u[k]]),$$

$$\text{and } \Omega = \cos(\xi[u[k]]) - \sin(\varphi[k]) \sin(\varphi[k-1]).$$

where and $\xi[u[k]] = \frac{\Delta T u[k-1]}{d(\mathbf{g}[k-1], \mathbf{0})}$ is the angular distance traveled and $d(\mathbf{g}[k-1], \mathbf{0})$ is the distance from the center of the sphere to $\mathbf{g}[k-1] = (\varphi[k-1], \lambda[k-1])$, which is recalculated every iteration. The states are latitude φ , longitude λ , current speed in the latitudinal direction v_φ , and current speed in the longitudinal direction v_λ . The currents v_φ and v_λ are initially set as 0, but are updated when a range measurement is available.

The model does not represent the AUV diving. This is not a problem for short dives but is an issue if a large change in depth takes a while to achieve. Pitch should be incorporated into the model if long dives are needed.

3.2.2 Observation Model

The observation model is described in this subsection. The observation, or measurement, model \mathbf{h} is used to model the range measurement from the location of the vehicle to the shore transducer. It is based on (3.3). The range measurement is the Euclidean distance $d(\mathbf{p}_1, \mathbf{p}_2)$ between locations \mathbf{p}_1 and \mathbf{p}_2 . The Euclidean distance between locations \mathbf{g}_1 and \mathbf{g}_2 expressed in geodetic coordinates is

$$\begin{aligned}
d_g(\mathbf{g}_1, \mathbf{g}_2) = & [(N(\varphi_1) + h_1 - \delta_1)^2 (\cos^2 \varphi_1 \cos^2 \lambda_1 + \cos^2 \varphi_1 \sin^2 \lambda_1) \\
& + (N(\varphi_2) + h_2 - \delta_2)^2 (\cos^2 \varphi_2 (\cos^2 \lambda_2 + \sin^2 \lambda_2)) \\
& - 2(N(\varphi_1) + h_1 - \delta_1)(N(\varphi_2) + h_2 - \delta_2) [\cos \varphi_1 \cos \varphi_2 (\cos \lambda_1 \cos \lambda_2 + \sin \lambda_1 \sin \lambda_2)] \\
& + [(1 - e^2)N(\varphi_1) + h_1 - \delta_1]^2 \sin^2 \varphi_1 \\
& + [(1 - e^2)N(\varphi_2) + h_2 - \delta_2]^2 \sin^2 \varphi_2 \\
& - 2[(1 - e^2)N(\varphi_1) + h_1 - \delta_1][(1 - e^2)N(\varphi_2) + h_2 - \delta_2] \sin \varphi_1 \sin \varphi_2]^{1/2} \quad (3.11)
\end{aligned}$$

which can be simplified as

$$\begin{aligned}
d_g(\mathbf{g}_1, \mathbf{g}_2) &= [(N(\varphi_1) + h_1 - \delta_1)^2 \cos^2 \varphi_1 + (N(\varphi_2) + h_2 - \delta_2)^2 \cos^2 \varphi_2 \\
&\quad - 2(N(\varphi_1) + h_1 - \delta_1)(N(\varphi_2) + h_2 - \delta_2)[\cos \varphi_1 \cos \varphi_2 \cos(\lambda_1 - \lambda_2)] \\
&\quad + [(1 - e^2)N(\varphi_1) + h_1 - \delta_1] \sin \varphi_1 - [(1 - e^2)N(\varphi_2) + h_2 - \delta_2] \sin \varphi_2]^2]^{1/2} \\
&= [\mu_1^2 \cos^2 \varphi_1 + \mu_2^2 \cos^2 \varphi_2 - 2\mu_1\mu_2[\cos \varphi_1 \cos \varphi_2 \cos(\lambda_1 - \lambda_2)] \\
&\quad + [\rho_1 \sin \varphi_1 - \rho_2 \sin \varphi_2]^2]^{1/2} \tag{3.12}
\end{aligned}$$

where $\mu_1 = (N(\varphi_1) + h_1 - \delta_1)$, $\mu_2 = (N(\varphi_2) + h_2 - \delta_2)$, $\rho_1 = [(1 - e^2)N(\varphi_1) + h_1 - \delta_1]$, and $\rho_2 = [(1 - e^2)N(\varphi_2) + h_2 - \delta_2]$.

Denote the distance from the AUV to the shore transducer as $d_g(\mathbf{g}_{AUV}, \mathbf{g}_T)$. For ease of notation, the $[k]$ is dropped. All values are at time k for the measurement model $\mathbf{h}(\mathbf{x}[k])$, which is

$$\begin{aligned}
\mathbf{h}(\mathbf{x}[k]) &= d_g(\mathbf{g}_{AUV}, \mathbf{g}_T) \tag{3.13} \\
&= [\mu_{AUV}^2 \cos^2 \varphi_{AUV} + \mu_T^2 \cos^2 \varphi_T \\
&\quad - 2\mu_{AUV}\mu_T[\cos \varphi_{AUV} \cos \varphi_T \cos(\lambda_{AUV} - \lambda_T)] \\
&\quad + [\rho_{AUV} \sin \varphi_{AUV} - \rho_T \sin \varphi_T]^2]^{1/2}
\end{aligned}$$

3.2.3 Rejection of Inaccurate Range Measurements

A method to reject an inaccurate range measurement is derived in this subsection. Range measurements will occasionally be inaccurate. To reject an inaccurate range measurement, a radius of error is calculated using variances from the EKF state estimate error covariance \mathbf{P} and measurement noise covariance \mathbf{R} . Measurements outside the radius of error are rejected. The radius of error r_e is one standard deviation away from the expected range measurement

since inaccurate range measurements are much larger than the true range. The radius of error is

$$r_e[k] = \sqrt{\sigma_{\varphi\varphi,m}^2[k] + \sigma_{\lambda\lambda,m}^2[k] + \sigma_{d_T}^2[k]} \quad (3.14)$$

where $\sigma_{\varphi\varphi,m}^2$ and $\sigma_{\lambda\lambda,m}^2$ are the \mathbf{P}_{11} and \mathbf{P}_{22} entries in the covariance \mathbf{P} , respectively. They are expressed in meters. The variance $\sigma_{d_T}^2$ is the only element of the covariance matrix \mathbf{R} and is the variance of the measurement noise in meters.

The variances $\sigma_{\varphi\varphi}^2$ and $\sigma_{\lambda\lambda}^2$ are in units of radians but are approximated in meters since range measurements are in meters. Denote the length in meters per degree latitude as m_φ and the length in meters per degree longitude as m_λ . The length of a degree, in meters, of latitude and longitude are approximated using the formula from the National Geospatial-Intelligence Agency ‘Length of a Degree of Latitude and Longitude’ calculator [28] are

$$m_\varphi = 111132.92 - 559.82 \cos(2\varphi) + 1.175 \cos(4\varphi) - 0.0023 \cos(6\varphi) \quad (3.15a)$$

$$m_\lambda = 111412.84 \cos(\varphi) - 93.5 \cos(3\varphi) + 0.118 \cos(5\varphi) \quad (3.15b)$$

The approximated variances of the latitude and longitude positions in meters are

$$\sigma_{\varphi\varphi,m}^2 = \sigma_{\varphi\varphi}^2 \left(\frac{180}{\pi} m_\varphi \right)^2 \quad (3.16a)$$

$$\sigma_{\lambda\lambda,m}^2 = \sigma_{\lambda\lambda}^2 \left(\frac{180}{\pi} m_\lambda \right)^2 \quad (3.16b)$$

where the subscript m corresponds to meters.

It is assumed that the noise models are independent normal distributions. Hence, the sum of the distributions is

$$\mathcal{N}(0, \sigma_{\varphi\varphi,m}^2 + \sigma_{\lambda\lambda,m}^2 + \sigma_{d_T}^2) = \mathcal{N}(0, \sigma_{\varphi\varphi,m}^2) + \mathcal{N}(0, \sigma_{\lambda\lambda,m}^2) + \mathcal{N}(0, \sigma_{d_T}^2) \quad (3.17)$$

and one standard deviation of (3.17) is r_e .

To accept or reject the range measurement, the expected measurement $d_{T,e}$ calculated via the Euclidean distance, is compared to the actual measurement d_T . If the absolute value of the difference is less than r_e , then the measurement is accepted; if not, it is rejected. The pseudocode is

Algorithm 1 Accept or Reject

```

1: procedure ACCEPTORREJECT
2:    $r_e \leftarrow$  radius of error in meters
3:   calculate expected range measurement and compare to actual:
4:    $d_{T,e} \leftarrow$  expected range measurement
5:    $d_T \leftarrow$  actual range measurement
6:   if  $|d_{T,e} - d_T| \leq r_e$  then
7:     return accept
8:   else
9:     return reject

```

3.3 The Extended Kalman Filter for Range Navigation

The EKF for range navigation is based on the kinematic model \mathbf{f} from (3.10) and measurement model \mathbf{h} from (3.13) proposed in Subsections 3.2.1 and 3.2.2. The EKF formulation has the same format as Section 2.4. The state $\mathbf{x}[k]$ and measurement $\mathbf{z}[k]$ vectors for the range navigation algorithm are formulated in this section. The states of the system are latitude φ , longitude λ , current in the latitudinal direction v_φ , and current in the longitudinal direction v_λ . The state vector is

$$\mathbf{x}[k] = \mathbf{f}(\mathbf{x}[k-1], k) + \boldsymbol{\omega}[k] \quad (3.18)$$

where \mathbf{f} is the kinematic model from (3.10).

A range measurement from the transducer on the AUV to the shore transducer is represented by the measurement vector

$$\mathbf{z}[k] = \mathbf{h}(\mathbf{x}[k]) + \boldsymbol{\nu}[k] \quad (3.19)$$

where \mathbf{h} is the measurement model from (3.13).

The state transition matrix \mathbf{F} and observation matrix \mathbf{H} are the Jacobians from (2.10). Due to the length of some of the elements in the Jacobians, the full Jacobians are shown in Appendix B. The EKF is initialized

$$\mathbf{x}[0|0] = \mathbb{E}[\mathbf{x}[0]] \quad (3.20a)$$

$$\mathbf{P}[0|0] = \mathbb{E}[(\mathbf{x}[0] - \mathbb{E}[\mathbf{x}[0]])(\mathbf{x}[0] - \mathbb{E}[\mathbf{x}[0]])^T] \quad (3.20b)$$

while \mathbf{Q} and \mathbf{R} are initialized based on how accurate the model and measurements are, respectively. The pseudocode for the EKF algorithm is

Algorithm 2 EKF for RangeNav

```

1: procedure RANGENAVEKF
2:    $\mathbf{P} \leftarrow$  Initialize error covariance
3:    $\mathbf{Q} \leftarrow$  Initialize process noise covariance
4:    $\mathbf{R} \leftarrow$  Initialize measurement covariance
5:    $v_\varphi \leftarrow$  Initialize latitudinal current
6:    $v_\lambda \leftarrow$  Initialize longitudinal current
7:   Loop to initialize navigation filter by acquiring GPS measurement before dive:
8:   if GPS is available then
9:     return initialized and exit loop
10:  else
11:    continue loop
12:  Loop EKF:
13:  if GPS is available then
14:    return position of AUV and update  $\mathbf{P}$ 
15:  else predict position of AUV:

```

```

16:      $\mathbf{x}[k|k-1] = \mathbf{f}(\mathbf{x}[k-1], k)$ 
17:      $\mathbf{P}[k|k-1] = \mathbf{F}[k]\mathbf{P}[k-1|k-1]\mathbf{F}[k]^\top + \mathbf{Q}$ 
18:     if Range measurement is available then
19:         AcceptOrReject
20:         if Accepted then EKF update step:
21:              $\mathbf{K}[k] = \mathbf{P}[k|k-1]\mathbf{H}[k]^\top(\mathbf{H}[k]\mathbf{P}[k|k-1]\mathbf{H}[k]^\top + \mathbf{R})^{-1}$ 
22:              $\mathbf{x}[k|k] = \mathbf{x}[k|k-1] + \mathbf{K}[k](z[k] - \mathbf{h}(\mathbf{x}[k]))$ 
23:              $\mathbf{P}[k|k] = (\mathbf{I} - \mathbf{K}[k]\mathbf{H}[k])\mathbf{P}[k|k-1]$ 
24:     return estimated states and covariance  $\mathbf{P}$ 

```

The EKF loop should iterate at the same rate that heading, depth, and speed are sampled. For the AUV used in this thesis, the heading, depth, and speed are sampled at a rate of 10Hz. Therefore, if GPS is not available, the AUV predicts its location every tenth of a second via dead reckoning. The update step occurs when a range measurement is available. Due to drops and occasional inaccurate measurements, the update step is not performed at a constant rate. The AUV is set to ping the shore transducer every 10 seconds, but it is not guaranteed to receive and accept a measurement every 10 seconds.

Chapter 4

Experimental Results and Performance Assessment

4.1 Experimental Apparatus

This section discusses the hardware used for range navigation along with experimental setup. The Virginia Tech 690s AUV, pictured in [Figure 4.1](#), was used for initial data collection. It has successfully been deployed and has completed several in-field missions. The 690s is a streamlined AUV with four independent control surfaces and a propeller at the stern. The AUV's specifications are listed in [Table 4.1](#).



(a) The Virginia Tech 690s AUV



(b) Field trial in Claytor Lake, VA

Figure 4.1: The Virginia Tech 690s AUV is shown out of water in Figure 4.1a and during a field trial in Figure 4.1b.

Table 4.1: The Virginia Tech 690s AUV Specifications

Symbol	Description
Displacement	61 lbs
Length	61 inches
Diameter	6.9 inches
Max Depth	500 meters
Communication	Iridium satcom, RF modem, Wi-Fi, acoustic modem
Navigation on surface	GPS
Navigation underwater	Inertially aided dead reckoning and range navigation
Computer	ODROID-U3
Operating System/Kernel	Gentoo 2.2/Linux 3.8.13

The 690s AUV has several sensors equipped, however only the ones used for range navigation are listed. The AUV's sensor specifications are listed in Table 4.2

Table 4.2: The Virginia Tech 690s Sensor Suite

Measurement	Sensor
Attitude	Microstrain 3DM-GX3-25 AHRS
Absolute Position	Linx RXM-GPS-R4 GPS receiver
Depth	Keller PA-30X pressure sensor
Range	Teledyne Benthos ATM-903 acoustic modem and transducer combination
Speed	Castle Creations motor controller reports RPM

The Microstrain 3DM-GX3-25 AHRS reports roll, pitch, yaw, linear accelerations, and angular rates. Only yaw is used for the proposed range navigation algorithm. The Linx RXM-GPS-R4 GPS receiver provides absolute position but accuracy is not specified on the data sheet. The Keller PA-30X pressure sensor has a $\pm 0.1\%$ full scale accuracy. The Teledyne Benthos ATM-903 acoustic modem and transducer combination, shown in Figure 4.2, acquires a range measurement and location from a remote transducer (shore transducer). The shore transducer is connected to a Universal Deck Box (UDB) that is located on the boat. A Castle Creations motor controller reports the propeller's RPM. Speed trials were conducted to map the speed of the propeller in RPM to the speed of the AUV in m/s. Assuming a linear relationship between the two, 910 RPM maps to approximately 1m/s. The propeller is a three-bladed propeller and the motor is a brushless DC motor.



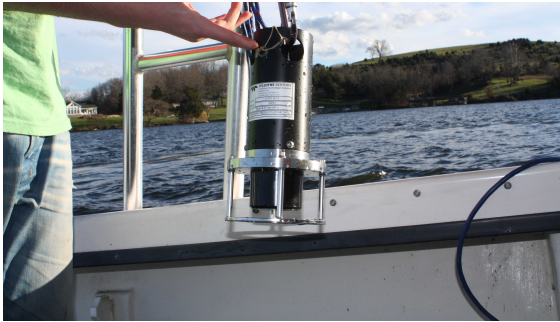
Figure 4.2: The 690s AUV contains a Teledyne Benthos ATM-903 acoustic modem (left) and transducer (right).

The UDB is pictured in Figure 4.3. The UDB-9400 contains a Benthos acoustic modem and connects to an AT-440-MF transducer, which operates between 16-21 kHz. The UDB updates its location (latitude and longitude) at a rate of 1 Hz from an external USGlobalSat BU-353 GPS receiver, which has a horizontal position accuracy of 10m 2D RMS. The depth of the transducer below the surface of the water is set as a constant value.



Figure 4.3: The Teledyne Benthos Universal Deck Box is pictured above. The top right plug connects to the shore transducer, the circular plug below the transducer plug is for power, and COM 1 is used for serial communication with a computer.

The UDB is located on a moving boat and is connected to an AT-440-MF transducer that is pictured in Figure 4.4a. The AT-440-MF transducer is referred to as the shore transducer in the rest of this thesis. The shore transducer is attached to a rope (shown in Figure 4.4b) that is tied to the side of a boat and hangs three meters below the surface of the water. The port COM 1 on the UDB connects to a shore laptop. The laptop has its GPS location updated at a rate of 1 Hz via an external USGlobalSat BU-353 GPS receiver. COM 1 is used to update the shore transducer location from the shore laptop.



(a) AT-440-MF Transducer (also referred to as shore transducer).



(b) The shore transducer is attached to a rope and shown hanging from the side of a boat.

Figure 4.4: The shore transducer is shown hanging from the side of a boat.

The 690s AUV is set to ping the shore transducer, which is attached to the UDB, every ten seconds using the ‘ATRXn’ (Range and Location) command. Several unsuccessful attempts were made to achieve range measurements faster than every ten seconds. The shortest time period recorded between range measurements from the 690s to the shore transducer was seven seconds, however this was not consistent. On average, it takes 10 seconds between range measurements. The shore transducer sends its location (latitude, longitude, and depth) when the 690s utilizes the ‘ATRXn’ command. For these tests, the transmit power level is set to -9 dB of attenuation and the acoustic bit rate is set to 800 bits/second.

4.2 Assessment of Range Measurements and Their Performance

This section describes the assessment of acquiring range measurements in the field. The 690s was deployed in two parts of Claytor Lake to acquire range measurements from the shore transducer attached to a moving boat. The goal of these trials was to find an environment where acoustic ranging performs well. Performance was assessed by determining the number of successful range measurements acquired out of the number of range measurement

attempts, and by determining the accuracy of the range measurements that were successfully acquired.

Visual inspection of the data is used to determine if a measurement is accurate. For example, the AUV is initially 30m away from the boat and then moves away from the boat. One should see the measured range increase roughly at the same rate that the AUV travels, which is approximately 1.25 m/s. Obvious outliers are identified easily. An operation area where acoustic ranging performs well can be used for range navigation.

Acoustic modem performance was assessed in the two locations of Claytor Lake shown in Figure 4.5. The white arrow in Figure 4.5 points to Claytor Dam.

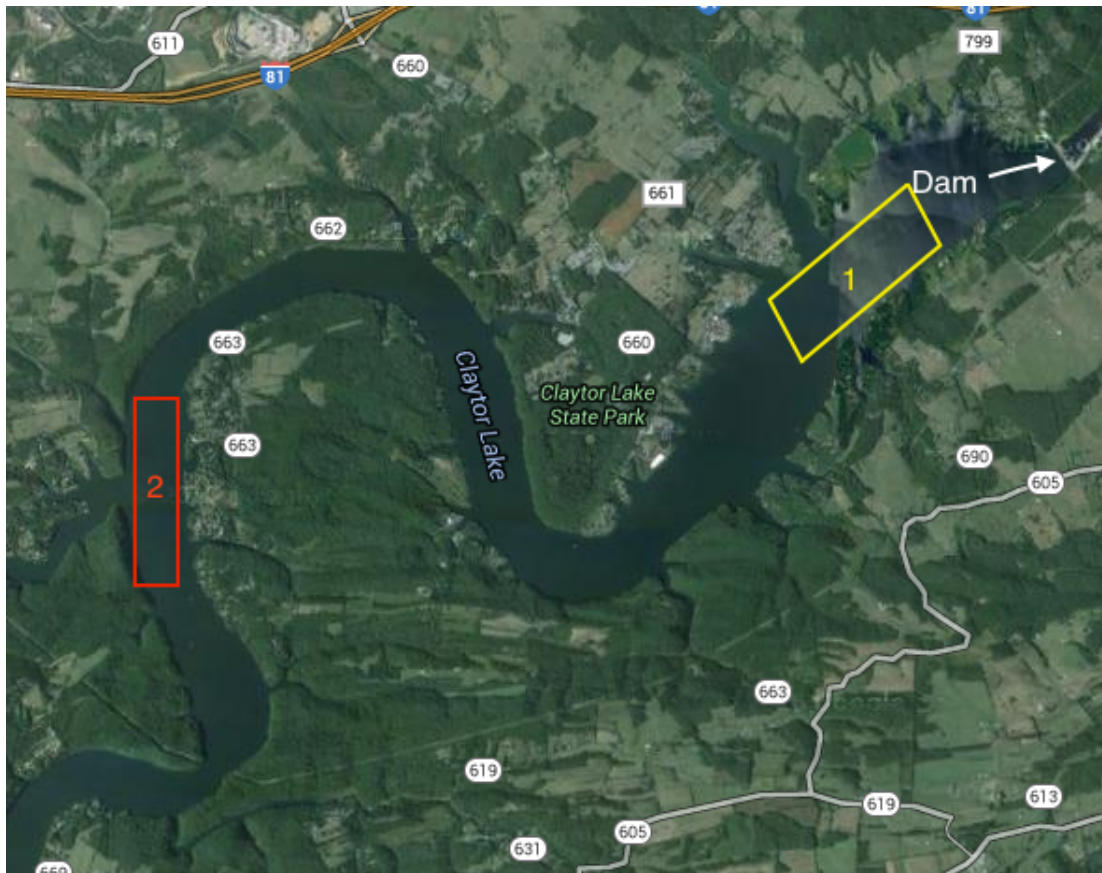


Figure 4.5: Claytor Lake is shown with the two outlined operation areas used for field trials. The satellite image of Claytor Lake was acquired from Google Maps.

The AUV was commanded in a straight-line trajectory for several three to five minute missions. In operation area 1, less than 20 range measurements were acquired during approximately 45 minutes of underwater missions. The large amount of range drops could be due to destructive noise or multipath from the nearby dam, however this assumption is not confirmed. In contrast, range measurement attempts were mostly successful in operation area 2, and most range measurements appeared to be accurate. The follow-on trial occurred in operation area 2.

4.3 Assessment of Navigation Performance Without Currents in Claytor Lake

The performance of the geodetic range navigation system is assessed in this section. The final estimated position of the AUV at surfacing was compared to the true position determined from GPS. The average error for four trials was 17.8m and considered an acceptable result.

AUV field trials were conducted on 8 January 2016 with the 690s in operation area 2 of Claytor Lake, VA. The goal was to collect the necessary data to implement a geodetic range navigation algorithm via post-processing prior to implementing the algorithm on the 690s. The UDB was located on a moving boat for these trials. The magnetic declination in this area is approximately -8.1 degrees. Four straight-line trajectories are evaluated in this section. Table 4.3 shows the mission specifications of each trial.

Table 4.3: Claytor Lake Mission Descriptions

Mission Number	Heading [°]	Speed [m/s]	Depth [m]	Time Underwater [s]
1	210	1.1	1.0	240
2	20	1.1	1.0	240
3	185	1.65	1.0	180
4	195	1.65	1.0	180

The GPS receiver used to measure the location of the UDB and boat has a 10 meter 2D RMS accuracy. Additionally, the transducer loosely swung from a 4m rope and the GPS receiver was not located directly above the transducer. The depth of the transducer for the UDB was set to a constant 3m depth below the water surface. Covariance matrices for the EKF are initialized in units of meters and meters/second but converted to units of radians and radians/second by using the information from (3.15). Variances in meters have the subscript m and variances in radians have the subscript r . The conversion from meters to radians is dependent on the latitude position. The variables m_φ and m_λ denote the length of a degree latitude and longitude in meters, respectively. The conversion from meters to radians is

$$\sigma_{\varphi\varphi,r}^2 = \sigma_{xx,m}^2 \left(\frac{1}{m_\varphi} \right)^2 \left(\frac{\pi}{180} \right)^2 \quad (4.1a)$$

$$\sigma_{\lambda\lambda,r}^2 = \sigma_{yy,m}^2 \left(\frac{1}{m_\lambda} \right)^2 \left(\frac{\pi}{180} \right)^2 \quad (4.1b)$$

$$\sigma_{v_\varphi v_\varphi,r}^2 = \sigma_{v_x v_x,m}^2 \left(\frac{1}{m_\varphi} \right)^2 \left(\frac{\pi}{180} \right)^2 \quad (4.1c)$$

$$\sigma_{v_\lambda v_\lambda,r}^2 = \sigma_{v_y v_y,m}^2 \left(\frac{1}{m_\lambda} \right)^2 \left(\frac{\pi}{180} \right)^2 \quad (4.1d)$$

The trajectories from Table 4.3 are shown in Figures 4.6, 4.8, 4.10, and 4.12. The dead reckoning trajectory of the AUV is shown in magenta. The trajectory based on the geodetic range navigation EKF is shown in green. The green x's represent when a range measurement is accepted. The white and red diamonds are the true starting and ending positions of the

AUV, respectively. GPS locations before and after diving are shown as red dots; jumps in GPS location occur in the beginning because 30 seconds are needed for the GPS receiver to generate an accurate position measurement after a warm start. The location of the UDB on the boat is shown in cyan; its initial position starts at the white triangle and ends at the red triangle. The operation area is plotted over a satellite image provided by the Google Maps API.

The acquired range measurements during the trajectories are show in Figures 4.7, 4.9, 4.11, and 4.13. Range measurements are shown at the times that they are acquired. Measurements that are accepted are represented by blue x's while rejected measurements are red x's. Inaccurate measurements were rejected by using algorithm 1. It is clear by visual inspection that the rejected range measurements are the outliers. It can be observed that range measurements are acquired approximately every ten seconds if they are not dropped or rejected. When a range measurement is received and accepted, the EKF update step is performed and the AUV corrects its position.



Figure 4.6: Mission 1 is illustrated above. The satellite image of Claytor Lake was acquired from Google Maps.

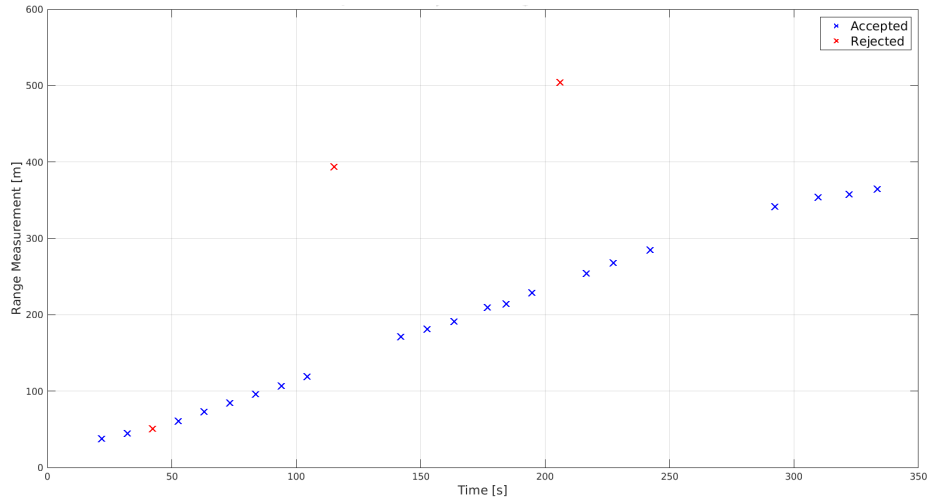


Figure 4.7: Range measurements from mission 1. 24 measurements are acquired and 3 are rejected. The rejection in the beginning could be due to a range measurement being received before the GPS receiver acquired an accurate measurement.

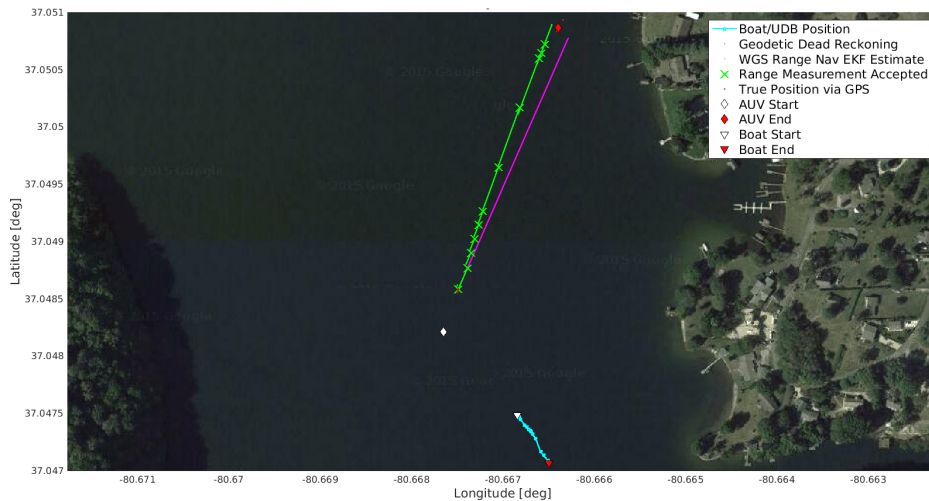


Figure 4.8: Mission 2 is illustrated above. The satellite image of the operation area was acquired from Google Maps.

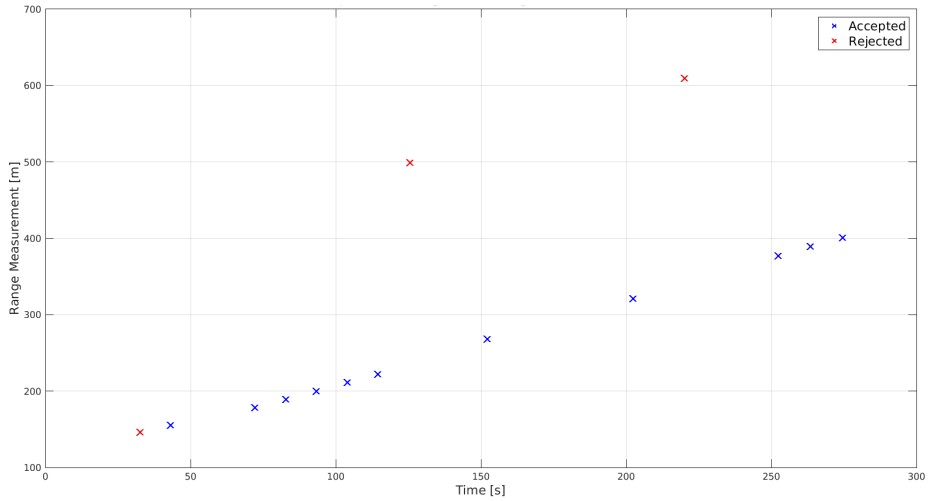


Figure 4.9: Range measurements from mission 2. 14 measurements are acquired and 3 are rejected. The rejection in the beginning could be due to a range measurement being received before the GPS receiver acquired an accurate measurement.

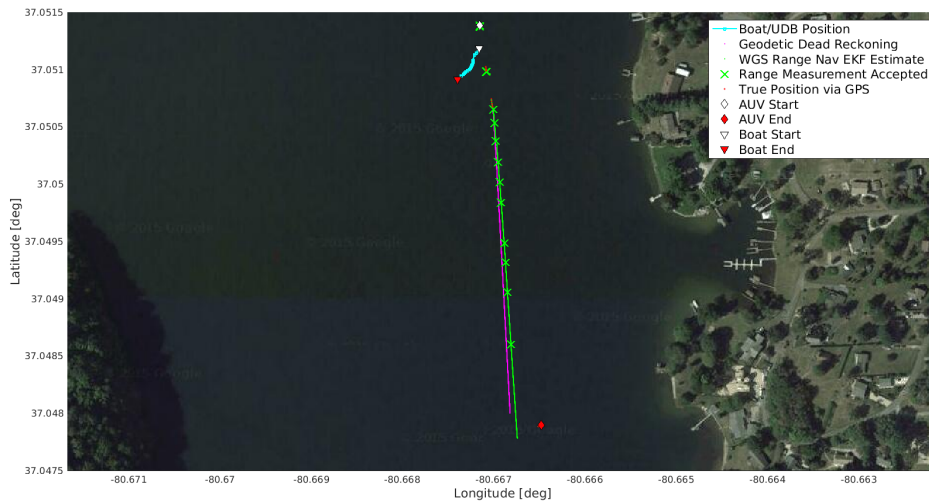


Figure 4.10: Mission 3 is illustrated above. The satellite image of the operation area was acquired from Google Maps.

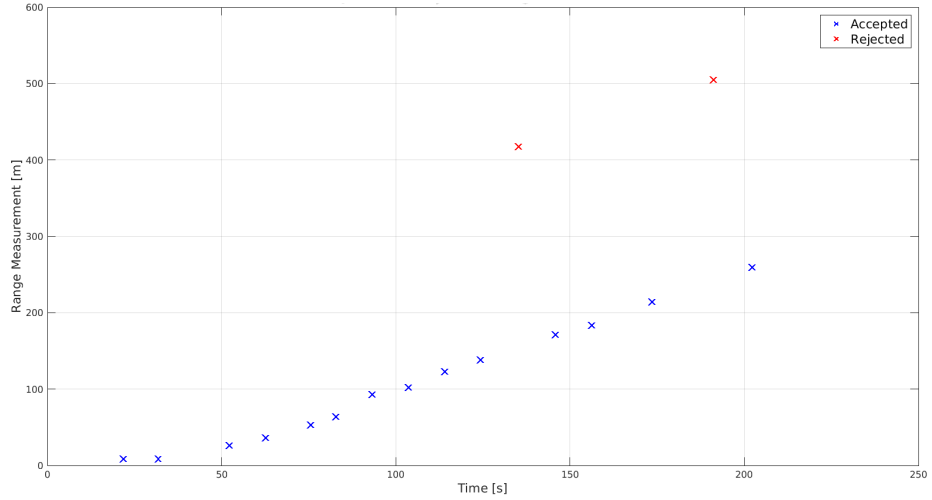


Figure 4.11: Range measurements from mission 3. 16 measurements are acquired and 2 are rejected.

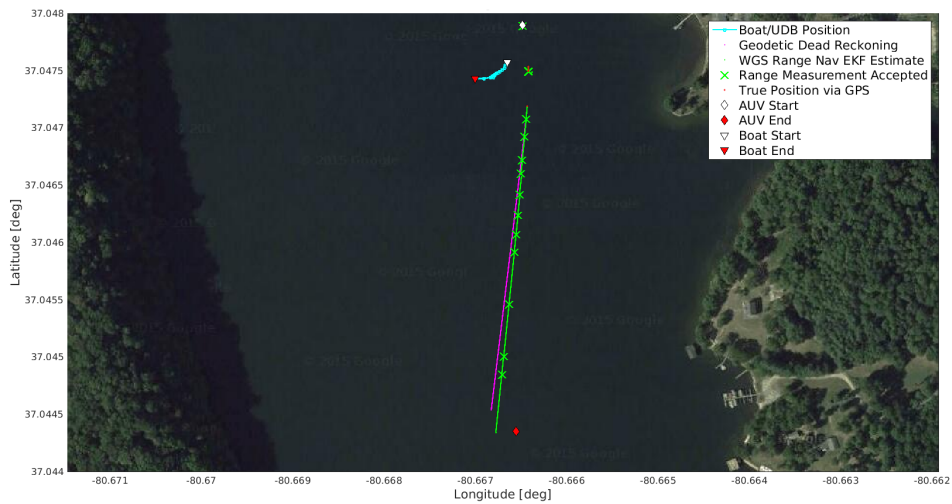


Figure 4.12: Mission 4 is illustrated above. The satellite image of the operation area was acquired from Google Maps.

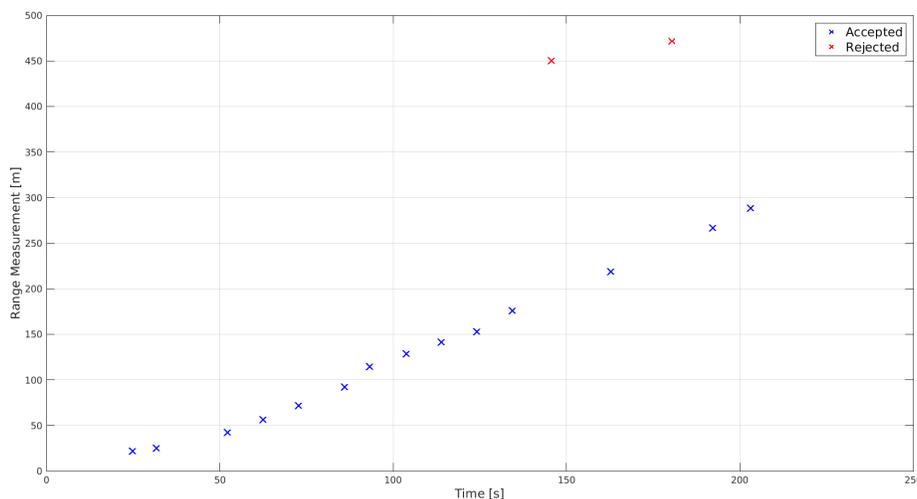


Figure 4.13: Range measurements from mission 4. 16 measurements are acquired and 2 are rejected.

By visual inspection it is clear that the EKF is correcting the AUV position throughout the trajectory. Table 4.4 shows the final estimated location of the vehicle, true final location, and the distance between the points in meters for each mission. The average distance is approximately 17.8 meters.

Table 4.4: Distance Errors from Claytor Lake Trials

Mission Number	Final Estimate [°]	True [°]	Distance [m]
1	(37.0482384, -80.6679173)	(37.0482297, -80.6676358)	25.0
2	(37.0508905, -80.6664695)	(37.0508641, -80.6663965)	7.1
3	(37.0477840, -80.6667408)	(37.0478831, -80.6665116)	23.13
4	(37.0442633, -80.6666989)	(37.0443503, -80.6665543)	16.07

Missions 2 and 4 are more accurate than missions 1 and 3. This could be due to the fact that the trajectories for missions 1 and 3 are close to being radial with the boat, which validates work from [1] stating that a trajectory radial with the beacon is not observable and produces results similar to dead reckoning. Additionally, results could be different due to compass bias in different directions. There are other sources of error as well. The shore

transducer is hanging from a rope and can sway while the boat moves. The GPS receiver on the boat was not located directly above the shore transducer.

Another method of evaluating the performance of the range navigation algorithm in geodetic coordinates is to compare it to the previously developed algorithm reported in [1] that operates in a local Cartesian NED coordinate system. The covariance matrices for the local range navigation algorithm are initialized using the same variances in meters and meters/second. The origin is set as the initial location of the boat and UDB. Mission 2 is compared. Both algorithms perform very similarly, but there are minute differences in the estimated position, which can be due to the error that arises when translating between units.

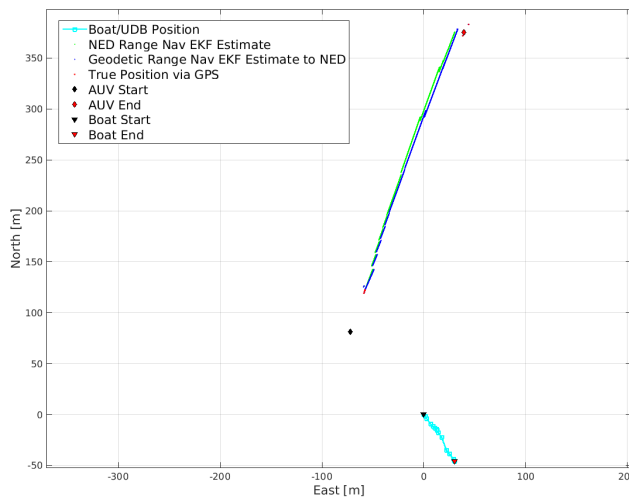


Figure 4.14: The local NED range navigation solution (green) is compared to the solution from the geodetic range navigation algorithm converted to NED (blue). Performance is similar.

Claytor Lake is a calm environment with almost no current. Section 4.4 shows algorithm performance in the Chesapeake Bay, which has significant currents. The current estimation performance is then evaluated.

4.4 Assessment of Navigation Performance with Currents in the Chesapeake Bay

The performance of the geodetic range navigation system including current estimation is assessed in this section. Position estimation is assessed in Subsection 4.4.2 and current estimation is assessed in Subsection 4.4.3. The final estimated position of the AUV at surfacing was compared to the true position determined from GPS. The average error for two trials was 21.53m and considered an acceptable result. To assess the performance of the range navigation algorithm in estimating currents, the EKF current estimate was compared with that provided by the National Oceanic and Atmospheric Administration's (NOAA) Tides and Currents at Sandy Point (38.3083° , -76.4550°) [29].

The field trials were conducted on 14 April 2016 and the operation area was near Solomons, MD. The data sets in this chapter were collected between 12:00 and 13:00 local time. Figure 4.15 shows the location of Sandy point relative to the operation area.



Figure 4.15: The operation area is outlined by the yellow box. The red x is the location of the Sandy Point current estimate. The satellite image of the operation area was acquired from Google Maps.

4.4.1 Experimental Setup Modifications

This subsection documents the modifications made to the experimental setup from Claytor Lake. The modified setup reduces some of the sources of error addressed from the Claytor Lake trials. The shore transducer was no longer attached to a rope; it was attached to an aluminum pole that mounts to the side of a boat (shown in Figure 4.16). This modification prevents the shore transducer from swaying while the boat is moving and keeps the transducer one meter below the water surface while the boat drifts. The GPS receiver that updates the location of the UDB and shore transducer was placed directly above the aluminum pole to reduce position uncertainty.



Figure 4.16: The shore transducer is shown mounted to the side of a boat that is out of the water. When the boat is in the water the shore transducer is one meter below the water's surface.

It was assumed that the altitude in the operation area is constant. To determine the altitude in the operation area, the GPS data from the AUV was recorded on the surface of the water and then averaged. The speed of sound for the acoustic modem was determined by Coppens' Equation (3.2). The salinity was measured with a hydrometer to be 11 parts per thousand. Surface temperature was measured by a depth sounder system that is attached to the boat. The propeller was changed for these trials and the RPM to m/s relation was instrumented again. 1150 RPM corresponded to approximately 1m/s.

4.4.2 Assessment of Position Estimation

Position estimation is assessed in this subsection. The geodetic range navigation algorithm was incorporated into the 690s software for these trials. However, the tidal current variances, $\sigma_{v_\varphi v_\varphi}^2$ and $\sigma_{v_\lambda v_\lambda}^2$, in the initial covariance matrices were initialized too small. Due to the significant currents in the Bay, the 690s drifted too fast and the range measurements were rejected. Without range measurements, the EKF trajectory followed the geodetic dead reckoning trajectory. Additionally, there was a compass bias due to improper AHRS calibration. After accounting for the miscalibration and slightly increasing the variances for the currents, the data set from the AUV was reprocessed to produce the trajectories in Figures 4.17 and 4.19. It should be noted that the 690s would have accepted range measurements and properly corrected its trajectory in real time if the covariance matrices were set properly and if the AHRS was calibrated properly.

Two trajectories are evaluated in this section. Table 4.5 shows the mission specifications of each trial. The description column contains the heading commanded and the length of time the AUV is commanded for in seconds.

Table 4.5: Chesapeake Bay Mission Descriptions

Mission Number	Description	Speed [m/s]	Depth [m]	Time Underwater [s]
CB1	250° for 250s 280° for 160s 330° for 90s 70° for 130s	1.36	1.5	630
CB2	270° for 230s 315° for 195s 250° for 125s 160° for 160s	1.36	1.5	734

The trajectories from Table 4.5 are shown in Figures 4.17 and 4.19. The dead reckoning trajectory of the AUV is shown in magenta. The trajectory based on the geodetic range navigation EKF is shown in green. The green x's represent when a range measurement is accepted. The white and red diamonds are the true starting and ending positions of the AUV, respectively. GPS locations before and after diving are shown as red dots. The location of the UDB on the boat is shown in cyan; its initial position starts at the white triangle and ends at the red triangle. The operation area is plotted over a satellite image provided by the Google Maps API.

The acquired range measurements during the trajectories are shown in Figures 4.18 and 4.20. Range measurements are shown at the times that they are acquired. Measurements that are accepted are represented by blue x's while rejected measurements are red x's. It is clear by visual inspection that the rejected range measurements are the outliers. Inaccurate measurements were rejected by using algorithm 1. It can be observed that range measurements are acquired approximately every ten seconds if they are not dropped or rejected. When a range measurement is received and accepted, the EKF update step is performed and the AUV corrects its position.

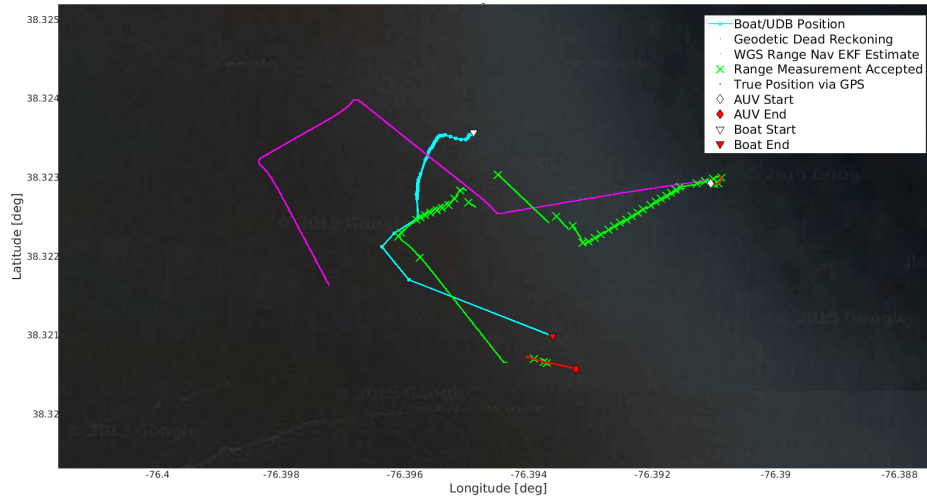


Figure 4.19: Mission CB2 is illustrated above. The satellite image of the operation area was acquired from Google Maps.

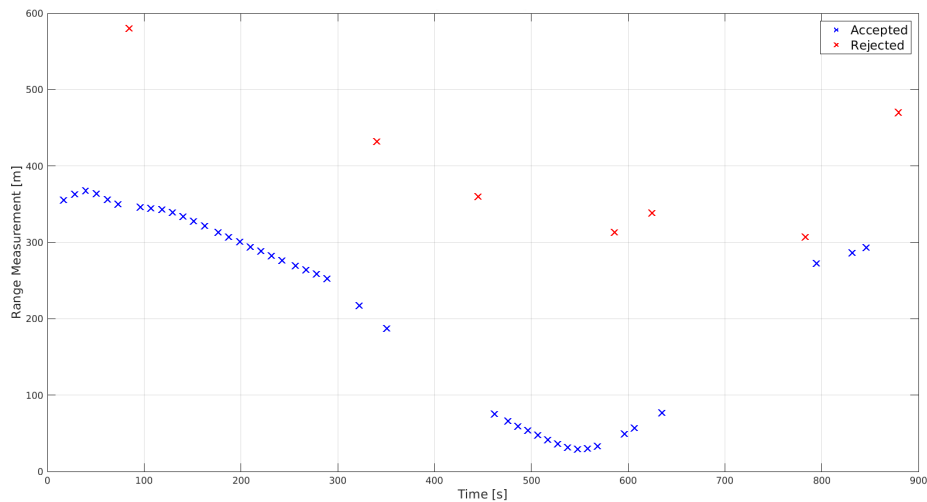


Figure 4.20: Range measurements from mission CB2. 50 measurements were acquired over a 900 second time period and 7 were rejected.

By visual inspection it is clear that the EKF is correcting the AUV position throughout the trajectory. Table 4.6 shows the final estimated location of the vehicle, true final location, and the distance between the points in meters for each mission. The average distance is approximately 21.53 meters.

Table 4.6: Distance Errors from Chesapeake Bay Trials

Mission Number	Final Estimate [°]	True [°]	Distance [m]
CB1	(38.3231179, -76.3936592)	(38.3230401, -76.3963035)	13.97
CB2	(38.3206553, -76.3943594)	(38.3207192, -76.3940361)	29.09

Missions CB1 was more accurate than mission CB2. This may have been due to the number of dropped range measurements at the end of CB2. The AUV went two and a half minutes without an accepted range measurement at the end of CB2 and did not receive measurements until it had surfaced. The boat being between the AUV and the shore transducer may have caused an increase in multipath, but this is not conclusive.

Another method of evaluating the performance of the range navigation algorithm in geodetic coordinates is to compare it to the previously developed algorithm reported in [1] that operates in a local Cartesian NED coordinate system. The covariance matrices for the local range navigation algorithm are initialized using the same variances in meters and meters/second. The origin is set as the initial location of the boat and UDB. Mission CB1 is compared. Both algorithms perform very similarly, again.

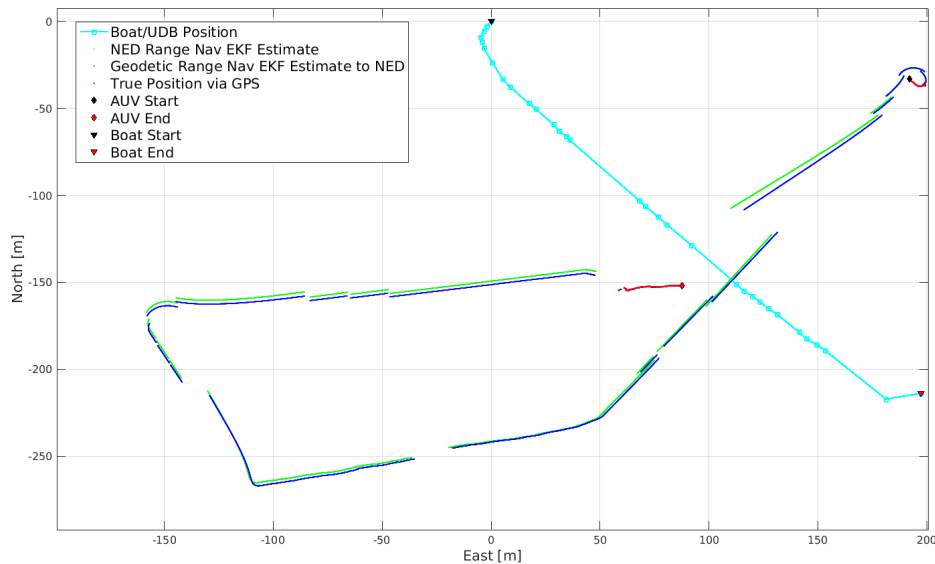


Figure 4.21: The local NED range navigation solution (green) is compared to the solution from the geodetic range navigation algorithm converted to NED (blue). Performance is similar.

4.4.3 Assessment of Current Estimation

This subsection assesses the performance of the current estimation. Since no ground truth was available, the current estimate from the geodetic range navigation algorithm is compared to an estimate created by NOAA at a nearby location. NOAA's Tides and Currents at Sandy Point [29] provides an estimate of the tidal current magnitude and direction during the time field trials were conducted. CB1 and CB2 were conducted at 1231 and 1252 local time. NOAA does not provide current estimates at those exact times, but a plot is provided that interpolates data between flood and ebb tides. The current speed estimates from NOAA are approximately 25cm/s and 27cm/s for CB1 and CB2, respectively. The direction given by NOAA is 125° . Another way to estimate the magnitude of the current is to take the final location of the dead reckoning solution and compute the distance to the location where the vehicle surfaced. The distance can then be divided by the total time between GPS fixes when

the vehicle dove and surfaced. By using the dead reckoning based method, the estimated current magnitudes are computed as approximately 39.97cm/s and 40.4cm/s.

The geodetic range navigation algorithm estimates latitudinal and longitudinal currents in units of rad/s. For plotting purposes, the values were converted to $^{\circ}$ /s. Figures 4.22 and 4.24 show the current estimates in $^{\circ}$ /s for CB1 and CB2, respectively. Estimates from the EKF need to be compared NOAA’s estimates, so the current estimate generated by the navigation algorithm is approximated in m/s. The latitude of the position measurement acquired from GPS when surfacing is used for the conversion. The latitudinal current is denoted as v_{North} and the longitudinal current is denoted as v_{East} in m/s. The estimated currents are compared to NOAA’s estimate and the estimate based on the final location of the dead reckoning trajectory. The plots are shown in Figures 4.23 and 4.25 for CB1 and CB2, respectively.

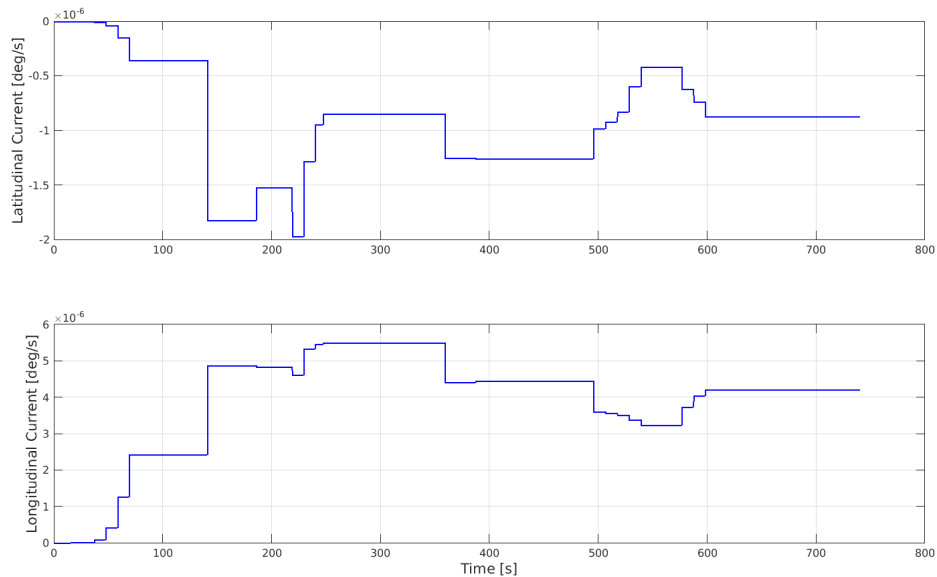


Figure 4.22: The latitudinal and longitudinal currents are estimated via the geodetic range navigation algorithm for mission CB1. They are presented in units of $^{\circ}$ /s.

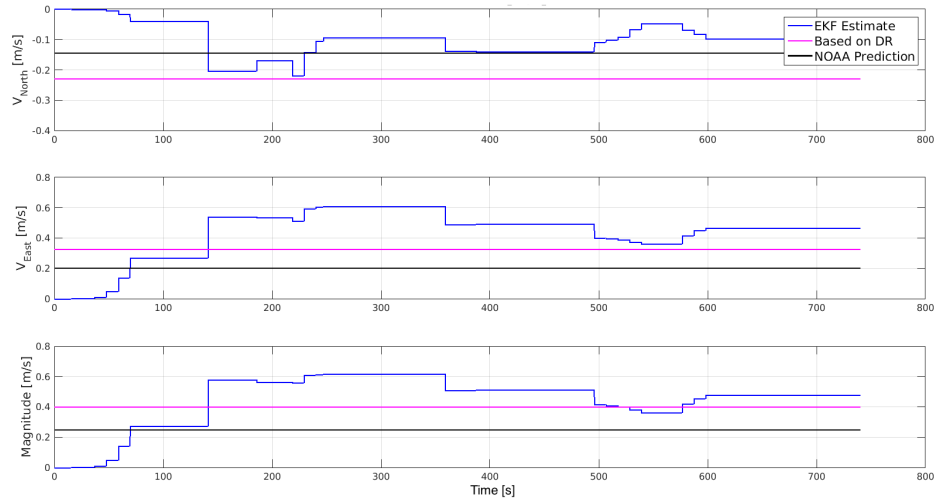


Figure 4.23: The latitudinal and longitudinal current estimates for CB1 are converted to units of m/s and compared against the NOAA current estimate and the estimate based on the final location of the dead reckoning trajectory.

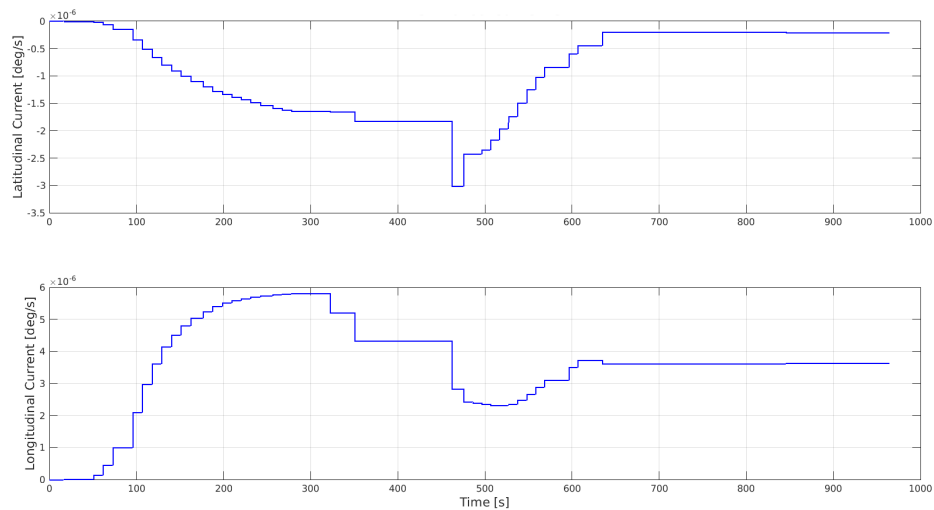


Figure 4.24: The latitudinal and longitudinal currents are estimated via the geodetic range navigation algorithm for mission CB2. They are presented in units of $^{\circ}/s$.

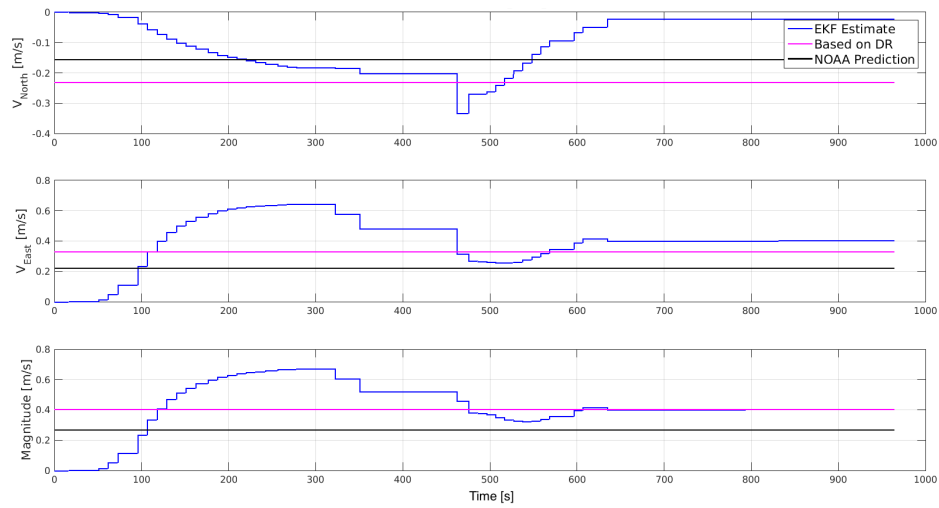


Figure 4.25: The latitudinal and longitudinal current estimates for CB2 are converted to units of m/s and compared against the NOAA current estimate and the estimate based on the final location of the dead reckoning trajectory.

It should be noted that the current estimated by the final dead reckoned position includes compass bias. The EKF current estimate also includes compass bias. The current estimate is reasonable and considered satisfactory. However, it cannot be compared to an instrumented current.

Chapter 5

Conclusions

This work proposes a range navigation algorithm in geodetic coordinates for AUVs. The main contribution of this work is the implementation of a range-based navigation system in geodetic coordinates for an AUV. The algorithm was implemented on the Virginia Tech 690s AUV and tested in real time. Additionally, a method to accept and reject range measurements is proposed. It is shown that the observability analysis in local Cartesian coordinates from [1] is still valid in geodetic coordinates except for at the poles. The proposed geodetic algorithm is compared to the local NED range navigation algorithm from [1] and the results are similar. The true trajectory underwater and the true current were not instrumented. The performance of the geodetic range navigation algorithm is based on the comparison with the true position when surfacing and currents estimated by NOAA.

In future work, the proposed geodetic algorithm can be extended to incorporate the case where the sensor noise is dependent on the state of the system. A kinematic model that incorporates pitch can be used to achieve more accurate results for deeper dives. The method of rejecting inaccurate range measurements can be revisited and a multi-hypothesis approach can be used. Since this work is not limited to using a single transponder, it can be

extended to use multiple transponders or other vehicles. It would be beneficial to instrument the position of the vehicle and currents to conduct a thorough performance evaluation. The addition of great-circle routes can be used for waypoint navigation since this algorithm takes into account Earth's curvature.

Bibliography

- [1] A. Gadre, *Observability Analysis in Navigation Systems with an Underwater Vehicle Application*. PhD dissertation, Virginia Tech, 2007.
- [2] T. Gode, “Long Baseline Ranging Acoustic Positioning System,” Master’s thesis, Virginia Tech, 2015.
- [3] A. Gadre and D. Stilwell, “Toward underwater navigation based on range measurements from a single location,” in *Robotics and Automation, 2004. Proceedings. ICRA '04. 2004 IEEE International Conference on*, vol. 5, pp. 4472–4477 Vol.5, April 2004.
- [4] A. Gadre and D. Stilwell, “Underwater navigation in the presence of unknown currents based on range measurements from a single location,” in *American Control Conference, 2005. Proceedings of the 2005*, pp. 656–661 vol. 1, June 2005.
- [5] A. Gadre and D. Stilwell, “A complete solution to underwater navigation in the presence of unknown currents based on range measurements from a single location,” in *Intelligent Robots and Systems, 2005. (IROS 2005). 2005 IEEE/RSJ International Conference on*, pp. 1420–1425, Aug 2005.
- [6] P.-M. Lee, B.-H. Jun, and Y.-K. Lim, “Review on underwater navigation system based on range measurements from one reference,” in *OCEANS 2008 - MTS/IEEE Kobe Techno-Ocean*, pp. 1–5, April 2008.

- [7] S. E. Webster, R. M. Eustice, H. Singh, and L. L. Whitcomb, “Advances in single-beacon one-way-travel-time acoustic navigation for underwater vehicles,” *The International Journal of Robotics Research*, vol. 31, no. 8, pp. 935–950, 2012.
- [8] M. Bayat, N. Crasta, A. P. Aguiar, and A. M. Pascoal, “Range-based underwater vehicle localization in the presence of unknown ocean currents: Theory and experiments,” *IEEE Transactions on Control Systems Technology*, vol. 24, pp. 122–139, Jan 2016.
- [9] Z. J. Harris and L. L. Whitcomb, “Preliminary feasibility study of cooperative navigation of underwater vehicles with range and range-rate observations,” in *OCEANS 2015 - MTS/IEEE Washington*, pp. 1–6, Oct 2015.
- [10] Y. T. Tan, R. Gao, and M. Chitre, “Cooperative path planning for range-only localization using a single moving beacon,” *IEEE Journal of Oceanic Engineering*, vol. 39, pp. 371–385, April 2014.
- [11] A. Bahr, J. J. Leonard, and A. Martinoli, “Dynamic positioning of beacon vehicles for cooperative underwater navigation,” in *2012 IEEE/RSJ International Conference on Intelligent Robots and Systems*, pp. 3760–3767, Oct 2012.
- [12] M. Fallon, J. Folkesson, H. McClelland, and J. Leonard, “Relocating underwater features autonomously using sonar-based slam,” *Oceanic Engineering, IEEE Journal of*, vol. 38, pp. 500–513, July 2013.
- [13] J. Folkesson, J. Leederkerken, R. Williams, A. Patrikalakis, and J. Leonard, “A feature based navigation system for an autonomous underwater robot,” in *Field and Service Robotics*, pp. 105–114, Springer, 2008.
- [14] H. Johannsson, M. Kaess, B. Englot, F. Hover, and J. Leonard, “Imaging sonar-aided navigation for autonomous underwater harbor surveillance,” in *Intelligent Robots and*

- Systems (IROS)*, 2010 IEEE/RSJ International Conference on, pp. 4396–4403, Oct 2010.
- [15] “Department of Defense World Geodetic System 1984,” tech. rep., National Imagery and Mapping Agency, 2000.
- [16] J. Farrell and M. Barth, *The Global Position System & Inertial Navigation*. McGraw-Hill, 1999.
- [17] T. I. Fossen, *Guidance and Control of Ocean Vehicles*. Chichester: Wiley, 1994.
- [18] R. W. Sinnott, “Virtues of the Haversine,” in *Sky and Telescope*, p. 159, Aug 1984.
- [19] “NOAA Latitude/Longitude Distance Calculator.” <http://www.nhc.noaa.gov/gccalc.shtml>. Accessed: 2016-05-01.
- [20] “Aviation Formulary V1.46.” <http://williams.best.vwh.net/avform.htm#LL>. Accessed: 2016-05-01.
- [21] R. J. Hijmans, E. Williams, and C. Vennes, “Spherical Trigonometry.” <https://cran.r-project.org/web/packages/geosphere/index.html>, Dec 2015.
- [22] “Calculate distance, bearing and more between Latitude/Longitude points.” <http://www.movable-type.co.uk/scripts/latlong.html>. Accessed: 2016-05-01.
- [23] S. Thrun, W. Burgard, and D. Fox, *Probabilistic Robotics (Intelligent Robotics and Autonomous Agents)*. The MIT Press, 2005.
- [24] K. V. Mackenzie, “Nine-term equation for sound speed in the oceans,” pp. 807–812, 1981.
- [25] A. B. Coppens, “Simple equations for the speed of sound in Neptunian waters,” in *The Journal of the Acoustical Society of America*, pp. 862–863, 1981.

- [26] M. Chitre, S. Shahabudeen, L. Freitag, and M. Stojanovic, “Recent advances in underwater acoustic communications & networking,” in *OCEANS 2008*, pp. 1–10, Sept 2008.
- [27] J. A. Catipovic and L. E. Freitag, “High data rate acoustic telemetry for moving rovs in a fading multipath shallow water environment,” in *Autonomous Underwater Vehicle Technology, 1990. AUV '90., Proceedings of the (1990) Symposium on*, pp. 296–303, Jun 1990.
- [28] “National Geospatial-Intelligence Agency Distance Calculators.” http://msi.nga.mil/NGAPortal/MSI.portal?_nfpb=true&_st=&_pageLabel=msi_portal_page_145&calcCode=03. Accessed: 2016-03-28.
- [29] “NOAA Tides and Currents at Sandy Point.” http://tidesandcurrents.noaa.gov/noaacurrents/Predictions?id=ACT5941_1&d=2016-04-14&r=1&t=am%2Fpm&u=2&tz=LST%2FLDT&threshold=1eEq&thresholdvalue=. Accessed: 2016-04-16.
- [30] I. Todhunter, *Spherical Trigonometry for the Use of Colleges and Schools*. Macmillan and Company, 1879.

Appendix A

Destination Latitude and Longitude

This appendix documents a derivation of (2.5). Given an initial point $\mathbf{g}_B = (\varphi_B, \lambda_B)$, sphere radius, angular distance traveled along a great-circle route, and initial heading, the destination point $\mathbf{g}_A = (\varphi_A, \lambda_A)$ is determined using spherical trigonometry [30]. Figure A.1 shows a sphere with points \mathbf{g}_A , \mathbf{g}_B , and the north pole. The points can be connected to form a triangle on the surface of a sphere. Spherical trigonometry is utilized so the spherical law of sines, spherical law of cosines, and the cotangent formula are used. It should be noted that the law of sines and the law of cosines for a triangle on a two-dimensional plane are different than the spherical law of sines and the spherical law of cosines for a triangle on the surface of a sphere.

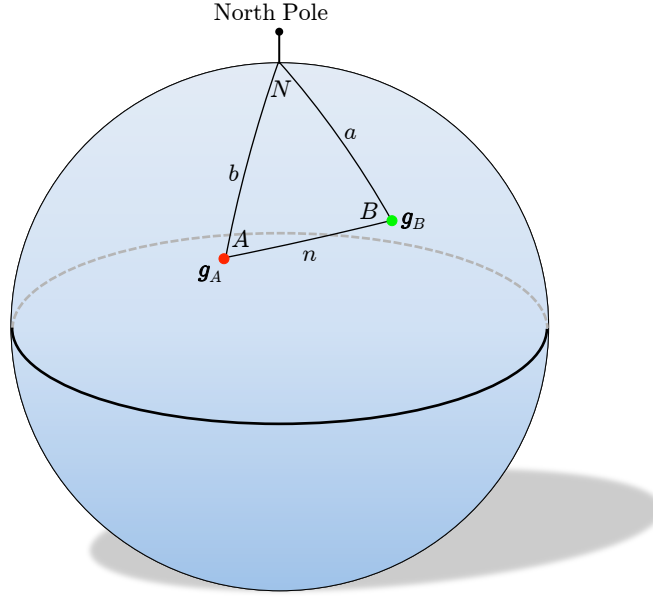


Figure A.1: The destination g_A is shown given the great-circle route from g_B .

By using the spherical law of sines and cosines, (2.5) is derived. The spherical law of cosines based on Figure A.1 is

$$\cos a = \cos n \cos b + \sin n \sin b \cos A \quad (\text{A.1})$$

$$\cos b = \cos n \cos a + \sin n \sin a \cos B \quad (\text{A.2})$$

$$\cos n = \cos a \cos b + \sin a \sin b \cos N \quad (\text{A.3})$$

and the spherical law of sines is

$$\frac{\sin A}{\sin a} = \frac{\sin B}{\sin b} = \frac{\sin N}{\sin n} \quad (\text{A.4})$$

where $a = 90^\circ - \varphi_B$, $b = 90^\circ - \varphi_A$, and $N = \lambda_A - \lambda_B$. Note that in spherical coordinates the latitude at the north pole is 0° and the latitude at the south pole is 180° .

The latitude at \mathbf{g}_A is based on the spherical law of cosines

$$\cos b = \cos n \cos a + \sin n \sin a \cos B \quad (\text{A.5})$$

$$\sin^{-1}(\cos b) = \sin^{-1}(\cos n \sin \varphi_B + \sin n \cos \varphi_B \cos B) \quad (\text{A.6})$$

$$90^\circ - b = \sin^{-1}(\cos n \sin \varphi_B + \sin n \cos \varphi_B \cos B) \quad (\text{A.7})$$

$$\boxed{\varphi_A = \sin^{-1}(\cos n \sin \varphi_B + \sin n \cos \varphi_B \cos B)} \quad (\text{A.8})$$

The longitude at \mathbf{g}_A is based on the spherical law of sines

$$\lambda_A = \lambda_B + N \quad (\text{A.9})$$

$$\lambda_A = \lambda_B + \sin^{-1}\left(\frac{\sin n \sin B}{\sin b}\right) \quad (\text{A.10})$$

however the domain of \sin^{-1} is between -1 and 1 so the cotangent formula

$$\cos a \cos B = \cot n \sin a - \cot N \sin B \quad (\text{A.11})$$

is used to modify (A.9) so \tan^{-1} is used instead of \sin^{-1} . The cotangent formula gives

$$\tan N = \frac{\sin B}{\frac{\sin a}{\tan n} - \cos a \cos B} \quad (\text{A.12})$$

$$\tan N = \frac{\sin B \sin n}{\sin a \cos n - \cos a \cos B \sin n} \quad (\text{A.13})$$

$$\tan N = \frac{\sin B \sin n \sin a}{\sin^2 a \cos n - \sin a \cos a \cos B \sin n} \quad (\text{A.14})$$

$$\tan N = \frac{\sin B \sin n \sin a}{\cos n - \cos n \cos^2 a - \sin a \cos a \cos B \sin n} \quad (\text{A.15})$$

$$\tan N = \frac{\sin B \sin n \sin a}{\cos n - \cos a(\cos a \cos n - \sin a \cos B \sin n)} \quad (\text{A.16})$$

$$\tan N = \frac{\sin B \sin n \sin a}{\cos n - \cos a \cos b} \quad (\text{A.17})$$

$$N = \tan^{-1}\left(\frac{\sin B \sin n \cos \varphi_B}{\cos n - \sin \varphi_B \varphi_A}\right) \quad (\text{A.18})$$

Hence, (A.9) is rewritten as

$$\boxed{\lambda_A = \lambda_B + \text{atan2}(\sin B \sin n \cos \varphi_B, \cos n - \sin \varphi_B \varphi_A)} \quad (\text{A.19})$$

where n is the angular distance traveled along the great-circle route. Denote the distance traveled as d and the sphere's radius as R . The angular distance traveled is $n = \frac{d}{R}$. The initial heading is denoted as B . The variables B and n are $\psi[k-1]$ and $\xi[u[k]]$ in (2.5), respectively.

Appendix B

Jacobians

This appendix documents the Jacobians used for the geodetic range navigation EKF in Section 3.3. The state transition matrix

$$\mathbf{F} = \begin{bmatrix} \frac{\partial f_1}{\partial \varphi[k-1]} & 0 & \Delta T & 0 \\ \frac{\partial f_2}{\partial \varphi[k-1]} & 1 & \frac{\partial f_2}{\partial v_\varphi[k-1]} & \Delta T \\ 0 & 0 & 1 & 0 \\ 0 & 0 & 0 & 1 \end{bmatrix}$$

where

$$f_1 = \sin^{-1}(\cos(\xi[u[k]]) \sin(\varphi[k-1]) + \cos(\varphi[k-1]) \cos(\psi[k-1]) \sin(\xi[u[k]])) + \Delta T v_\varphi[k-1]$$

$$f_2 = \lambda[k-1] + \text{atan2}(\cos(\varphi[k-1]) \sin(\psi[k-1]) \sin(\xi[u[k]]),$$

$$\cos(\xi[u[k]] - \sin(\varphi[k]) \sin(\varphi[k-1])) + \Delta T v_\lambda[k-1]$$

The observation matrix

$$\mathbf{H} = \begin{bmatrix} \frac{\partial h_1}{\partial \varphi_{AUV}} & \frac{\partial h_1}{\partial \lambda_{AUV}} & 0 & 0 \end{bmatrix}$$

where

$$\begin{aligned} h_1 = & [\mu_{AUV}^2 \cos^2 \varphi_{AUV} + \mu_T^2 \cos^2 \varphi_T \\ & - 2\mu_{AUV}\mu_T [\cos \varphi_{AUV} \cos \varphi_T \cos(\lambda_{AUV} - \lambda_T)] \\ & + [\rho_{AUV} \sin \varphi_{AUV} - \rho_T \sin \varphi_T]^2]^{1/2} \end{aligned}$$

$\mu_{AUV} = (N(\varphi_{AUV}) + h_{AUV} - \delta_{AUV})$, $\mu_T = (N(\varphi_T) + h_T - \delta_T)$, $\rho_{AUV} = [(1 - e^2)N(\varphi_{AUV}) + h_{AUV} - \delta_{AUV}]$, and $\rho_T = [(1 - e^2)N(\varphi_T) + h_T - \delta_T]$.